Event-Triggered Adaptive Fault-Tolerant Synchronization Tracking Control for Multiple 6-DOF Fixed-Wing UAVs

Zhang, Boyang; Sun, Xiuxia; Liu, Shuguang; Lv, Maolong; Deng, Xiongfeng

DOI
10.1109/TVT.2021.3129267

Publication date
2022

Document Version
Final published version

Published in
IEEE Transactions on Vehicular Technology

Event-Triggered Adaptive Fault-Tolerant Synchronization Tracking Control for Multiple 6-DOF Fixed-Wing UAVs

Boyang Zhang, Xiuxia Sun, Shuguang Liu, Maolong Lv, and Xiongfeng Deng

***Abstract*—In contrast with most existing results concerning unmanned aerial vehicles (UAVs) wherein two-degree or only attitude/longitudinal dynamics are considered, this article proposes an event-triggered cooperative synchronization fault-tolerant control (FTC) methodology for multiple fixed-wing UAVs whose dynamics are six-degree-of-freedom (DOF) with twelf-state-variables subject to actuator faults, modeling uncertainties, and external disturbances. More precisely, an event-triggering mechanism is devised to determine the time instants of updating control signals, which reduces the signal transmission burden, while saving on system resources. The Zeno phenomenon is excluded in the sense of guaranteeing that the time between two consecutive switchings is lower bounded by a positive constant. The actuator faults as well as the network induced errors are handled via the bound estimation approach and some well-defined smooth functions. By strict Lyapunov arguments, all closed-loop signals are proved to be semi-globally uniformly ultimately bounded (SGUUB) and the synchronization tracking errors of speed and attitude converge to a residual set around origin whose size can be made arbitrarily small through selecting appropriate design parameters.**

***Index Terms*—Event-triggered adaptive control, fault-tolerant control (FTC), backstepping, six-degree-of-freedom (DOF) fixed-wing unmanned aerial vehicles (UAVs).**

NOMENCLATURE

ϕ_i	Roll angle
ϕ_r	Reference command of ϕ_i
ψ_i	Yaw angle
ψ_r	Reference command of ψ_i
ρ	Air density
θ_i	Pitch angle
θ_r	Reference command of θ_i
m_i	Vehicle mass
p_i	Angular velocity in X of body fixed frame
q_i	Angular velocity in Y of body fixed frame
r_i	Angular velocity in Z of body fixed frame
u_i	Linear speed in X of body fixed frame
V_i	Total speed in body fixed frame
v_i	Linear speed in Y of body fixed frame
V_r	Reference command of V_i
w_i	Linear speed in Z of body fixed frame
α_i	Attack angle
$\bar{c}_i$	Mean aerodynamic chord
$\bar{q}_i$	Dynamic pressure
β_i	Sideslip angle
$\boldsymbol{\delta}_i$	Flight control surface
$\boldsymbol{S}(\bullet)$	Skew-symmetric matrix
δ_{ai}	Aileron angular deflection
δ_{ei}	Elevator angular deflection
δ_{ri}	Rudder angular deflection
$\lambda_{\max}(\bullet)$	Maximum eigenvalue of a matrix
$\lambda_{\min}(\bullet)$	Minimum eigenvalue of a matrix
$\Re^m$	Real m-vector
$\Re^{m\times n}$	Real $m \times n$ matric
$\mathrm{SO}(3)$	Third-order Special Orthogonal group
b_i	Wingspan
S_i	Wing surface area
$\boldsymbol{\omega}_i$	Non-inertial expression of angular velocity
$\boldsymbol{\varphi}_i$	Attitude described by Euler angles
$\boldsymbol{\varphi}_r$	Reference command of $\boldsymbol{\varphi}_i$
$\boldsymbol{d}_{\omega i}$	External disturbances in angular velocity
$\boldsymbol{d}_{vi}$	External disturbances in speed
$\boldsymbol{F}_i$	Aerodynamics force
$\boldsymbol{g}$	Gravity acceleration
$\boldsymbol{J}_i$	Inertia tensor
$\boldsymbol{N}_i$	Aerodynamics moment
$\boldsymbol{p}_i$	Inertial position
$\boldsymbol{T}_i$	Thrust vector along x body axis
$\boldsymbol{v}_i$	Non-inertial expression of linear speed

Manuscript received December 15, 2020; revised May 5, 2021 and September 1, 2021; accepted November 14, 2021. Date of publication November 19, 2021; date of current version January 20, 2022. This work was supported in part by the Key Project of Natural Science Research of Universities in Anhui Province under Grant KJ2020A0344, in part by the University Synergy Innovation Program of Anhui Province under Grant GXXT-2020-069, and in part by the Pre-research Project of National Natural Science Foundation of Anhui Polytechnic University under Grant Xjky2020020. The review of this article was coordinated by Prof. A. Pedro Aguiar. *(Corresponding author: Maolong Lv.)*

Boyang Zhang, Xiuxia Sun, and Shuguang Liu are with the Department of Equipment Management, and Unmanned Aerial Vehicle Engineering, Air Force Engineering University, Xian 710051, China (e-mail: boyang_530@163.com; gcxysxx@126.com; dawny_liu@126.com).

Maolong Lv is with the College of Air Traffic Control and Navigation, Air Force Engineering University, Xi'an 710051, China, and also with the Delft Center for Systems and Control, Delft University of Technology, 2628 CD Delft, Netherlands (e-mail: m.lyu@tudelft.nl).

Xiongfeng Deng is with the Anhui Key Laboratory of Electric Drive and Control, Anhui Polytechnic University, Wuhu 241000, China (e-mail: fate2015zero@163.com).

Digital Object Identifier 10.1109/TVT.2021.3129267

I. Introduction

RESEARCH on cooperative flight of multiple fixed-wing unmanned aerial vehicles (UAVs) has attracted increasing attention recently in lots of applications due to the advantages such as mission cooperation, flexibility and cost effectiveness [1], [2]. In general, the coordinated control problem has been investigated in several aspects, including the task assignment and motion re-coordination for UAVs in a group [3], and synchronous tracking of speed and attitude for UAV formation [4] (that is to achieve $V_i \to V_r$, $V_i \to V_j$, $(\phi_i, \theta_i, \psi_i) \to (\phi_r, \theta_r, \psi_r)$ and $(\phi_i, \theta_i, \psi_i) \to (\phi_j, \theta_j, \psi_j)$). In particular, the distributed control strategy has particularly been attached tremendous attentions due to the fact that global information is no longer required in control design, while preserving closed-loop stability [5], [6]. Driven by the emerging distributed cooperative control research on multiple UAVs, some results have appeared in [7]–[10]. To list a few, [7] presented a distributed cooperative control design for networked UAVs against actuator faults and model uncertainties, while maintaining the synchronization of flight attitude. In [8], for longitudinal synchronization tracking of multiple UAVs, a distributed cooperative fault-tolerant controller was proposed in the presence of input saturation. Based on swarm intelligence, [9] proposed a distributed model predictive approach for coordination control of multiple UAVs. In [10], with path-following vector fields, the UAV group achieves a circular motion around the target, while rendering the course angles and speeds to converge to the vector field-specified values.

However, it is worth mentioning that all aforementioned methods [7]–[10] are performed based on the assumption that either the UAV dynamics can be simplified to be two-degree models [9], [10], or only attitude/longitudinal models are taken into account [7], [8]. Such a model simplification unavoidably lowers the system description precision. In other words, the dynamics in [7]–[10] cannot accurately describe the actual UAV system due to the fact that the fixed-wing UAV system is actually an nonlinear dynamic model with six-degree-of-freedom (DOF) with twelf-state-variables, which can be decomposed into rotational and translational dynamics respectively. Therefore, the motivation of investigation on six-DOF UAV dynamics naturally arises.

Moreover, note that the cooperative flight in aforementioned studies is achieved within continuous-time framework. Whereas, for multi-UAV system, being actually a networked control system with various links such as sensors, controllers and actuators, limited bandwidth of signal transmission as a main concerning influences the system performances [5], [6]. Especially in cooperative flight of UAVs, lots of signal transmissions are required. Therefore, the traditional periodical updating of control signals is likely to cause transmission channel congestion. In addition, when implemented within the framework of continuous-time control, the control updating is executed at every fixed sampling period no matter whether it is necessary or not, which would cause overloading of transmission burden in some cases. Above phenomenons will be more apparent as the number of UAVs grows. As a result, the periodic sampled

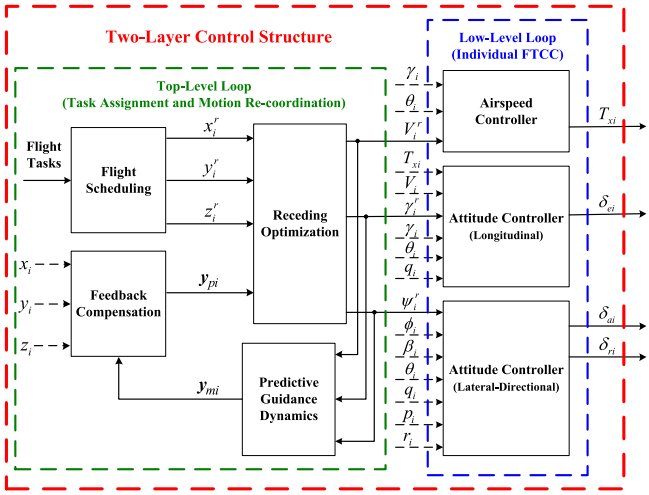

Fig. 1. Two-layer control structure of distributed UAV system.

controls are inappropriate for multi-UAV system. The main concern is the control design with event-triggered mechanism, which functions as an important solution to reducing the signal transmission frequency.

The idea of event-triggered control is firstly presented in [11]. Different from traditional periodic or time-triggered control, the signal transmission between different modules relies on a state-, input-, or output dependent triggering condition, which significantly reduces the transmission burden. This technique has been successfully applied to UAV systems. Based on distributed model predictive control scheme, the event-triggered mechanism was developed in [9], [12], [13] for cooperative path following of multi-UAVs. In [14], an event-triggered output feedback control method was presented for UAV system over cognitive radio networks. Further, [15] proposed an event-triggered based attitude control for UAV system against external disturbances. Although effective performances are obtained in aforementioned results [9], [12]–[15] with event-triggered mechanism, two problems are worth mentioning: the first is that, the event-triggered controls were proposed only for single UAV in [14], [15]. The second problem is that, even if the multi-UAVs were considered in [9], [12], [13], only two-degree model was discussed, being far from the actual UAV system. Considering the six-DOF UAVs, the complex dynamics makes the event-triggered control design more challenging. Therefore, the novel event-triggered control scheme for six-DOF multi-UAV system should be further exploited.

In formation flight of multiple UAVs, actuator faults have adverse impacts on the safety of the individual UAV but also induce the instability of the overall networked UAVs [16], [17]. To avoid the catastrophes induced by the actuator faults, the fault-tolerant cooperative control (FTCC) is progressively investigated for multiple UAVs in recent years, where following the two-layer control structure of distributed UAV system in Fig. 1, the individual FTCC is most investigated to compensate the fault effects for the faulty UAV. In [8], [18], the FTCC schemes were developed for multi-UAVs in the longitudinal

plane within a distributed control design. [7], [19]–[22] further investigated the FTCC for attitude dynamics of multi-UAVs in the presence of actuator faults. However, it should be noted that the FTCC methods presented in [7], [8], [18]–[22] were developed to only regulate the longitudinal motions and attitude dynamics of multi-UAVs, with no consideration of six-DOF dynamics. Regarding the six-DOF multi-UAV system, the strongly nonlinear dynamics of UAV makes the distributed FTCC design more complex and the aforementioned results can not be directly extended to the synchronization tracking of speed and attitude for multiple six-DOF UAVs. Therefore, more new and effective FTCC scheme should be further developed.

Motivated by above discussions, the main contribution of our paper is three-fold below:

• In comparison with the existing results which are concentrated on two-degree model [9], [10], longitudinal motion [8], [18] and attitude dynamics [7], [19]–[22], [31], [32] this study considers the distributed cooperative control for multi-UAVs where six-DOF UAV dynamics is considered subject to actuator faults, modeling uncertainties and external disturbances.

• Compared with the event-triggered control schemes which regulate on the single UAV [14], [15] or the two-degree model of multi-UAVs [9], [12], [13], this paper develops the distributed event-triggered control for six-DOF multi-UAVs, where the event-triggering mechanisms are introduced in translational and rotational subsystems respectively for each UAV, which considerably reduces the signal transmission load.

• Unlike most of the studies dealing with the control of UAV flight [3], [9]–[12], [23], [24], adaptive backstepping method is used together with the neural network approximation, bound estimation approach and well-defined smooth functions to accurately estimate and compensate the actuator faults, external disturbances and model uncertainties in the same time with the obtaining of global stability.

The rest of paper is organized as follows. In Section II, the UAV dynamics, actuator fault model, graph theory, and control objective are presented. Section III gives the details of event-triggered adaptive control design and stability analysis. Section IV shows the simulation results, and Section V draws the conclusions.

II. Problem Formulation and Preliminaries

A. UAV Kinematics and Dynamics

Consider a team of N identical fixed wing UAVs. Using Newton-Euler convention, the full six-DOF dynamics of the ith UAV (see Fig. 2), is given by [23], [24]

$$\dot{\boldsymbol{p}}_i = \boldsymbol{R}_1(\boldsymbol{\varphi}_i)\boldsymbol{v}_i, \tag{1}$$

$$\dot{\boldsymbol{v}}_i = -\boldsymbol{S}(\boldsymbol{\omega}_i)\boldsymbol{v}_i + \frac{\boldsymbol{T}_i}{m_i} + \boldsymbol{R}_1^{\mathrm{T}}(\boldsymbol{\varphi}_i)\boldsymbol{g} + \frac{\boldsymbol{F}_i}{m_i} + \boldsymbol{d}_{vi}, \tag{2}$$

$$\dot{\boldsymbol{\varphi}}_i = \boldsymbol{R}_2^{-1}(\boldsymbol{\varphi}_i)\boldsymbol{\omega}_i, \tag{3}$$

$$\boldsymbol{J}_i\dot{\boldsymbol{\omega}}_i = -\boldsymbol{\omega}_i \times \boldsymbol{J}_i\boldsymbol{\omega}_i + \boldsymbol{N}_i + \boldsymbol{C}_i\boldsymbol{\delta}_i + \boldsymbol{J}_i\boldsymbol{d}_{\omega i}, \tag{4}$$

where $\boldsymbol{p}_i = [x_i, y_i, z_i]^{\mathrm{T}}$ denotes the inertial position, $\boldsymbol{v}_i = [u_i, v_i, w_i]^{\mathrm{T}}$ is the non-inertial (body fixed frame coordinates) expression of the linear speed, $\boldsymbol{\varphi}_i = [\phi_i, \theta_i, \psi_i]^{\mathrm{T}}$ represents the attitude described by Euler angles, $\boldsymbol{\omega}_i = [p_i, q_i, r_i]^{\mathrm{T}}$ is the non-inertial expression of the angular velocity. Moreover, $\boldsymbol{T}_i = [T_{xi}, 0, 0]^{\mathrm{T}}$ denotes the thrust vector along x body axis, $\boldsymbol{\delta}_i = [\delta_{ai}, \delta_{ei}, \delta_{ri}]^{\mathrm{T}}$ is the control surface, where δ_{ei}, δ_{ai}, δ_{ri} represent the deflection of elevator, aileron and rudder respectively, m_i is the vehicle mass, $\boldsymbol{g} = [0, 0, g_z]^{\mathrm{T}}$ is the gravity acceleration in inertia frame, $\boldsymbol{d}_{vi} \in \Re^3$ and $\boldsymbol{d}_{\omega i} \in \Re^3$ are the unknown bounded external disturbances, $\boldsymbol{J}_i$ is the inertia tensor with the symmetric $x-z$ plane of which expression is

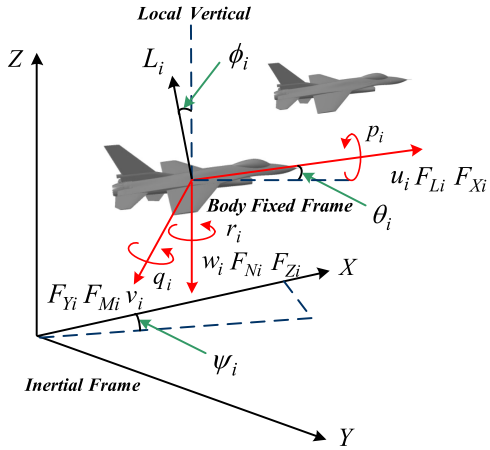

Fig. 2. Dynamical behavior of six-DOF UAV model.

$$\boldsymbol{J}_i = \begin{bmatrix} J_{xxi} & 0 & -J_{xzi} \\ 0 & J_{yyi} & 0 \\ -J_{zxi} & 0 & J_{zzi} \end{bmatrix}. \tag{5}$$

Besides, $\boldsymbol{R}_1(\boldsymbol{\varphi}_i) \in \mathrm{SO}(3)$ is the rotation matrix transforming the body frame coordinates to inertial axis coordinates and the matrix $\boldsymbol{R}_2(\boldsymbol{\varphi}_i) \in \Re^{3\times 3}$ maps the time derivative of the Euler angles to the non-inertial expression of the angular velocity. Both matrices are given as follows:

$$\boldsymbol{R}_1(\boldsymbol{\varphi}_i) = \begin{bmatrix} c_{\psi i}c_{\theta i} & -s_{\psi i}s_{\phi i}+c_{\psi i}s_{\theta i}s_{\phi i} & s_{\psi i}s_{\phi i}+c_{\psi i}s_{\theta i}c_{\phi i} \\ s_{\psi i}c_{\theta i} & c_{\psi i}c_{\phi i}+s_{\psi i}s_{\theta i}s_{\phi i} & -c_{\psi i}s_{\phi i}+s_{\psi i}s_{\theta i}c_{\phi i} \\ -s_{\theta i} & c_{\theta i}s_{\phi i} & c_{\theta i}c_{\phi i} \end{bmatrix}$$

$$\boldsymbol{R}_2(\boldsymbol{\varphi}_i) = \begin{bmatrix} 1 & 0 & -s_{\psi i} \\ 0 & c_{\psi i} & s_{\psi i}c_{\theta i} \\ 0 & -s_{\theta i} & c_{\psi i}c_{\theta i} \end{bmatrix}, \tag{6}$$

where s_a and c_a stand for $\sin(a)$ and $\cos(a)$ functions respectively. The aerodynamics force $\boldsymbol{F}_i = [F_{Xi}, F_{Yi}, F_{Zi}]^{\mathrm{T}}$ and moment $\boldsymbol{N}_i = [F_{Li}, F_{Mi}, F_{Ni}]^{\mathrm{T}}$ are calculated by means of aerodynamic coefficients:

$$\boldsymbol{F}_i = \bar{q}_i S_i \boldsymbol{R}_3^{-1}(\alpha_i, \beta_i)[-C_{Di}, C_{Yi}, -C_{Li}]^{\mathrm{T}}, \tag{7}$$

$$\boldsymbol{N}_i = \bar{q}_i S_i [b_i C'_{li}, \bar{c}_i C'_{Mi}, b_i C'_{ni}]^{\mathrm{T}}, \tag{8}$$

where $\alpha_i = \arctan(w_i/u_i)$ and $\beta_i = \arcsin(u_i/v_i)$ denote the attack angle and sideslip angle respectively. The dynamic pressure $\bar{q}_i = \frac{1}{2}\rho V_i^2$ is a function of V_i, which is the total speed in body fixed frame. Air density ρ, wingspan b_i, wing surface area S_i and mean aerodynamic chord $\bar{c}_i$ are constant parameters. The

transformation matrix $\boldsymbol{R}_3(\alpha_i, \beta_i)$ is

$$\boldsymbol{R}_3(\alpha_i, \beta_i) = \begin{bmatrix} c_{\alpha i}c_{\beta i} & s_{\beta i} & s_{\alpha i}c_{\beta i} \\ -c_{\alpha i}s_{\beta i} & c_{\beta i} & -s_{\alpha i}s_{\beta i} \\ -s_{\alpha i} & 0 & c_{\alpha i} \end{bmatrix}. \tag{9}$$

And $C_{Di}, C_{Yi}, C_{Li}, C'_{li}, C'_{Mi}$, and C'_{ni} are the dimensionless coefficients in force/moment expressions, of which corresponding detailed descriptions are shown in [23]. The control effectiveness matrix is defined as

$$\boldsymbol{C}_i = \begin{bmatrix} \bar{q}_i S_i b_i c_{l\delta ai} & 0 & \bar{q}_i S_i b_i c_{l\delta ri} \\ 0 & \bar{q}_i S_i \bar{c}_i c_{m\delta ei} & 0 \\ \bar{q}_i S_i b_i c_{n\delta ai} & 0 & \bar{q}_i S_i b_i c_{n\delta ri} \end{bmatrix}. \tag{10}$$

B. Control-Oriented Model With Actuator Faults and Modeling Uncertainties

According to [23], [24], the whole system can be decomposed into two interconnected subsystems, i.e., translational kinematics (2) and rotational kinematics (3)-(4). Then the controller for each subsystem is designed independently for each UAV.

1) Translational Kinematics: From (2), the time derivative of V_i is:

$$\dot{V}_i = \frac{\boldsymbol{v}_i^{\mathrm{T}}\dot{\boldsymbol{v}}_i}{V_i} = \frac{\boldsymbol{v}_i^{\mathrm{T}}}{V_i}(-\boldsymbol{S}(\boldsymbol{w}_i)\boldsymbol{v}_i + \frac{\boldsymbol{T}_i}{m_i} + \boldsymbol{R}_1^{\mathrm{T}}(\boldsymbol{\varphi}_i)\boldsymbol{g} + \frac{\boldsymbol{F}_i}{m_i} + \boldsymbol{d}_{vi}). \tag{11}$$

Based on (11), the thrust is extracted and using the property $\boldsymbol{v}_i^{\mathrm{T}}\boldsymbol{S}(\boldsymbol{w}_i)\boldsymbol{v}_i = 0$, it holds that

$$\dot{V}_i = \frac{u_i T_{xi}}{m_i V_i} + \frac{\boldsymbol{v}_i^{\mathrm{T}}}{V_i}\left(\boldsymbol{R}_1^{\mathrm{T}}(\boldsymbol{\varphi}_i)\boldsymbol{g} + \frac{\boldsymbol{F}_i}{m_i} + \boldsymbol{d}_{vi}\right). \tag{12}$$

Remark 1: From (12), even if there are no direct controls for speed components v_i and w_i, it is still controllable to point $\boldsymbol{v}_i$ in a desired direction by controlling V_i, α_i and β_i.

During operation, the thrust possibly suffers from actuator faults, modeled by [22]

$$T_{xi} = \rho_{Ti}T_{xi0} + T_{xif}, \tag{13}$$

where T_{xi0} is the designed control input, ρ_{Ti} is the unknown actuator efficiency factor satisfying $0 \le \rho_{Ti} \le 1$ and T_{xif} is the bounded unknown stuck fault or bias fault. Note that (13) implies the following four cases:

1) $\rho_{Ti} = 1$ and $T_{xif} = 0$. This means the fault-free case.

2) $0 < \rho_{Ti} < 1$ and $T_{xif} = 0$. This indicates the partial loss of effectiveness.

3) $\rho_{Ti} = 1$ and $T_{xif} \neq 0$. This indicates the bias fault.

4) $\rho_{Ti} = 0$ and $T_{xif} \neq 0$. This means that T_{xi} is stuck at bounded time-varying function T_{xif}.

Then with the actuator faults (13), the dynamics of (12) is described as

$$\dot{V}_i = \frac{u_i\rho_{Ti}T_{xi0}}{m_i V_i} + \frac{u_i T_{xif}}{m_i V_i} + \frac{\boldsymbol{v}_i^{\mathrm{T}}}{V_i}\left(\boldsymbol{R}_1^{\mathrm{T}}(\boldsymbol{\varphi}_i)\boldsymbol{g} + \frac{\boldsymbol{F}_i}{m_i} + \boldsymbol{d}_{vi}\right). \tag{14}$$

Note that the accurate information of $\boldsymbol{F}_i$ cannot be known a prior due to the coefficient uncertainties [25], [26]. In this sense, $\boldsymbol{F}_i$ is decomposed into a known component $\boldsymbol{F}_{i0}$ and an uncertain one $\Delta\boldsymbol{F}_i$. Therefore, the speed kinematics is reformulated as

$$\dot{V}_i = \frac{u_i\rho_{Ti}T_{xi0}}{m_i V_i} + \frac{u_i T_{xif}}{m_i V_i} + \frac{\boldsymbol{v}_i^{\mathrm{T}}}{V_i}\left(\boldsymbol{R}_1^{\mathrm{T}}(\boldsymbol{\varphi}_i)\boldsymbol{g} + \frac{\boldsymbol{F}_{i0}}{m_i} + \boldsymbol{\Delta}_{vi} + \boldsymbol{d}_{vi}\right). \tag{15}$$

where $\boldsymbol{\Delta}_{vi} = \Delta\boldsymbol{F}_i/m_i$.

2) Rotational Kinematics: From (3)-(4), the dynamical attitude motion in inertial reference frame is rewritten as

$$\dot{\boldsymbol{\varphi}}_i = \boldsymbol{R}_2^{-1}(\boldsymbol{\varphi}_i)\boldsymbol{\omega}_i, \tag{16}$$

$$\dot{\boldsymbol{\omega}}_i = \boldsymbol{J}_i^{-1}\boldsymbol{S}(\boldsymbol{J}_i\boldsymbol{\omega}_i) + \boldsymbol{J}_i^{-1}\boldsymbol{N}_i + \boldsymbol{J}_i^{-1}\boldsymbol{C}_i\boldsymbol{\delta}_i + \boldsymbol{d}_{\omega i}. \tag{17}$$

Considering the coefficient uncertainties [27], $\boldsymbol{J}_i^{-1}\boldsymbol{S}(\boldsymbol{J}_i\boldsymbol{\omega}_i)$ is decomposed into a known component $\boldsymbol{J}_{i0}^{-1}\boldsymbol{S}(\boldsymbol{J}_{i0}\boldsymbol{\omega}_i)$ and an uncertain one $\Delta\boldsymbol{J}_i^{-1}\boldsymbol{S}(\boldsymbol{J}_i\boldsymbol{\omega}_i)$. Similarly, $\boldsymbol{J}_i^{-1}\boldsymbol{N}_i$ is composed by a known part $\boldsymbol{J}_{i0}^{-1}\boldsymbol{N}_{i0}$ and an uncertain one $\Delta\boldsymbol{J}_i^{-1}\boldsymbol{N}_i$. Also, $\boldsymbol{J}_i^{-1}\boldsymbol{C}_i$ consists of a known component $\boldsymbol{J}_{i0}^{-1}\boldsymbol{C}_{i0}$ and an uncertain one $\Delta\boldsymbol{J}_i^{-1}\boldsymbol{C}_i$. Then the angular velocity model (17) is reformulated as

$$\begin{aligned}\dot{\boldsymbol{\omega}}_i = {} & \boldsymbol{J}_{i0}^{-1}\boldsymbol{S}(\boldsymbol{J}_{i0}\boldsymbol{\omega}_i) + \Delta\boldsymbol{J}_i^{-1}\boldsymbol{S}(\boldsymbol{J}_i\boldsymbol{\omega}_i) + \boldsymbol{J}_{i0}^{-1}\boldsymbol{N}_{i0} + \Delta\boldsymbol{J}_i^{-1}\boldsymbol{N}_i \\ & + \left(\boldsymbol{J}_{i0}^{-1}\boldsymbol{C}_{i0} + \Delta\boldsymbol{J}_i^{-1}\boldsymbol{C}_i\right)\boldsymbol{\delta}_i + \boldsymbol{d}_{\omega i}.\end{aligned} \tag{18}$$

During flight, the flight control surfaces inevitably suffers from actuator faults, which are considered as [7]

$$\delta_{ji} = \rho_{\delta ji}\delta_{ji0} + \delta_{jif} \tag{19}$$

where δ_{ji0} is the jth applied control input with $j = \{a, e, r\}$, $\rho_{\delta ji}$ is the unknown actuator efficiency factor satisfying $0 \le \rho_{\delta ji} \le 1$, and δ_{jif} is the bounded unknown stuck fault or bias fault. Consider that (19) satisfies the similar cases as (13) in the following.

1) $\rho_{\delta ji} = 1$ and $\delta_{jif} = 0$. This refers to the fault-free case.

2) $0 < \rho_{\delta ji} < 1$ and $\delta_{jif} = 0$. This means the partial loss of effectiveness.

3) $\rho_{\delta ji} = 1$ and $\delta_{jif} \neq 0$. This indicates the bias fault.

4) $\rho_{\delta ji} = 0$ and $\delta_{jif} \neq 0$. This means that δ_{ji} is stuck at bounded time-varying function δ_{jif}.

For the simplicity of presentation, the actuator fault model (19) is formulated by

$$\boldsymbol{\delta}_i = \boldsymbol{\rho}_{\delta i}\boldsymbol{\delta}_{i0} + \boldsymbol{\delta}_{if}, \tag{20}$$

where $\boldsymbol{\delta}_{i0} = [\delta_{ai0}, \delta_{ei0}, \delta_{ri0}]^{\mathrm{T}}$, $\boldsymbol{\rho}_{\delta i} = \mathrm{diag}\{\rho_{\delta ai}, \rho_{\delta ei}, \rho_{\delta ri}\}$, $\boldsymbol{\delta}_{if} = [\delta_{aif}, \delta_{eif}, \delta_{rif}]^{\mathrm{T}}$.

In the presence of actuator faults, the dynamic model of angular velocity can be formulated by

$$\dot{\boldsymbol{\omega}}_i = \boldsymbol{J}_{i0}^{-1}\boldsymbol{S}(\boldsymbol{J}_{i0}\boldsymbol{\omega}_i) + \boldsymbol{J}_{i0}^{-1}\boldsymbol{N}_{i0} + \boldsymbol{J}_{i0}^{-1}\boldsymbol{C}_{i0}\boldsymbol{\rho}_{\delta i}\boldsymbol{\delta}_{i0} + \boldsymbol{\Delta}_{\omega i} + \boldsymbol{d}_{\omega i}, \tag{21}$$

where $\boldsymbol{\Delta}_{\omega i} = \Delta\boldsymbol{J}_i^{-1}\boldsymbol{S}(\boldsymbol{J}_i\boldsymbol{\omega}_i) + \Delta\boldsymbol{J}_i^{-1}\boldsymbol{N}_i + \Delta\boldsymbol{J}_i^{-1}\boldsymbol{C}_i\boldsymbol{\delta}_i + \boldsymbol{J}_{i0}^{-1}\boldsymbol{C}_0(\boldsymbol{\delta}_i)\boldsymbol{\delta}_{if}$ is the lumped uncertainties induced by the actuator faults and modeling uncertainties.

Assumption 1 [28]: For $\forall t > 0$, it is supposed that $\|\Delta\boldsymbol{J}_i^{-1}\boldsymbol{C}_i\boldsymbol{\rho}_{\delta i}(\boldsymbol{J}_{i0}^{-1}\boldsymbol{C}_{i0})^{-1}\|_\infty < 1$ and $\partial\boldsymbol{\Delta}_{\omega i}/\partial\boldsymbol{\delta}_{i0} + \boldsymbol{J}_{i0}^{-1}\boldsymbol{C}_{i0}\boldsymbol{\rho}_{\delta i} \neq 0$.

Assumption 2 [29]: There exists a positive constant $g_{i,\min}$ such that $\lambda_{\min}(\boldsymbol{J}_{i0}^{-1}\boldsymbol{C}_{i0}\boldsymbol{\rho}_{\delta i}(\boldsymbol{J}_{i0}^{-1}\boldsymbol{C}_{i0})^{\mathrm{T}}) \geq g_{i,\min}$.

Remark 2: Assumptions 1-2 substantially guarantee the controllability of angular velocity dynamics (21), which implies that there still exists sufficient control action $\boldsymbol{\delta}_{i0}$ even in the presence of actuator faults for each UAV. Note that $g_{i,\min}$ is only used for analysis and not required a priori.

Remark 3: Considering that $\boldsymbol{\Delta}_{\omega i}$ involves the control signal $\boldsymbol{\delta}_{i0}$, if neural networks are used to approximate $\boldsymbol{\Delta}_{\omega i}$, the algebraic loops inevitably exists. To break the algebraic loops, the low-pass filter technique can be employed to filter $\boldsymbol{\delta}_{i0}$ [30]. Then $\boldsymbol{\Delta}_{\omega i} = \boldsymbol{\Delta}'_{\omega i} + \boldsymbol{l}_{\omega i}$, where $\boldsymbol{l}_{\omega i} \in \Re^{3\times 1}$ is the filtering error. At this point, the angular velocity kinematics can be described by

$$\begin{aligned}\dot{\boldsymbol{\omega}}_i = {} & \boldsymbol{J}_{i0}^{-1}\boldsymbol{S}\left(\boldsymbol{J}_{i0}\boldsymbol{\omega}_i\right) + \boldsymbol{J}_{i0}^{-1}\boldsymbol{N}_{i0} + \boldsymbol{J}_{i0}^{-1}\boldsymbol{C}_{i0}\boldsymbol{\rho}_{\delta i}\boldsymbol{\delta}_{i0} \\ & + \boldsymbol{\Delta}'_{\omega i} + \boldsymbol{l}_{\omega i} + \boldsymbol{d}_{\omega i}. \end{aligned} \tag{22}$$

C. Neural Network Approximation

As the universal approximation property, the RBFNNs are employed in this paper to compensate the modeling uncertainties [19], [21], [33]. Denote $\boldsymbol{\Theta}_{vi} = [\boldsymbol{v}_i^{\mathrm{T}}, \boldsymbol{\varphi}_i^{\mathrm{T}}, \boldsymbol{\omega}_i^{\mathrm{T}}, \boldsymbol{\delta}_{i0}^{\mathrm{T}}]^{\mathrm{T}} \in \Re^{12}$ and $\boldsymbol{\Theta}_{\omega i} = [\boldsymbol{v}_i^{\mathrm{T}}, \boldsymbol{\varphi}_i^{\mathrm{T}}, \boldsymbol{\omega}_i^{\mathrm{T}}, \boldsymbol{\delta}_{i0}^{\mathrm{T}}]^{\mathrm{T}} \in \Re^{12}$. For unknown continuous terms $\boldsymbol{\Delta}_{vi}(\boldsymbol{\Theta}_{vi}) = [\Delta_{vi1}, \Delta_{vi2}, \Delta_{vi3}]^{\mathrm{T}}$ and $\boldsymbol{\Delta}'_{\omega i}(\boldsymbol{\Theta}_{\omega i}) = [\Delta'_{\omega i1}, \Delta'_{\omega i2}, \Delta'_{\omega i3}]^{\mathrm{T}}$, there exist RBFNNs such that

$$\begin{aligned}\Delta_{vij}\left(\boldsymbol{\Theta}_{vi}\right) &= \boldsymbol{W}_{vij}^{*\mathrm{T}}\boldsymbol{\varsigma}_{vij}\left(\boldsymbol{\Theta}_{vi}\right) + \tau_{vij}\left(\boldsymbol{\Theta}_{vi}\right), \\ \Delta'_{\omega ij}\left(\boldsymbol{\Theta}_{\omega i}\right) &= \boldsymbol{W}_{\omega ij}^{*\mathrm{T}}\boldsymbol{\varsigma}_{\omega ij}\left(\boldsymbol{\Theta}_{\omega i}\right) + \tau_{\omega ij}\left(\boldsymbol{\Theta}_{\omega i}\right), \end{aligned} \tag{23}$$

where $j = 1, 2, 3$, $\tau_{vij}(\boldsymbol{\Theta}_{vi}) \in \Re$ and $\tau_{\omega ij}(\boldsymbol{\Theta}_{\omega i}) \in \Re$ are the bounded approximation errors. $\boldsymbol{W}_{vij}^{*} \in \Re^{M\times 1}$ and $\boldsymbol{W}_{\omega ij}^{*} \in \Re^{M\times 1}$ are idealized weight matrixes with M nodes. $\boldsymbol{\varsigma}_{vij}(\boldsymbol{\Theta}_{vi}) = [\varsigma_{vij}^1(\boldsymbol{\Theta}_{vi}), \ldots, \varsigma_{vij}^M(\boldsymbol{\Theta}_{vi})]^{\mathrm{T}} \in \Re^M$ and $\boldsymbol{\varsigma}_{\omega ij}(\boldsymbol{\Theta}_{\omega i}) = [\varsigma_{\omega ij}^1(\boldsymbol{\Theta}_{\omega i}), \ldots, \varsigma_{\omega ij}^M(\boldsymbol{\Theta}_{\omega i})]^{\mathrm{T}} \in \Re^M$ are known vectors consisted Gaussian basis functions $\varsigma_{vij}^l(\boldsymbol{\Theta}_{vi})$ and $\varsigma_{\omega ij}^l(\boldsymbol{\Theta}_{\omega i})$, $l = 1, \ldots, M$, commonly selected as the following exponential form:

$$\begin{aligned}\varsigma_{vij}^l\left(\boldsymbol{\Theta}_{vi}\right) &= \exp\left[-\frac{\left(\boldsymbol{\Theta}_{vi} - \boldsymbol{\Upsilon}_{vi}\right)^{\mathrm{T}}\left(\boldsymbol{\Theta}_{vi} - \boldsymbol{\Upsilon}_{vi}\right)}{\kappa_{vi}^2}\right], \\ \varsigma_{\omega ij}^l\left(\boldsymbol{\Theta}_{\omega i}\right) &= \exp\left[-\frac{\left(\boldsymbol{\Theta}_{\omega i} - \boldsymbol{\Upsilon}_{\omega i}\right)^{\mathrm{T}}\left(\boldsymbol{\Theta}_{\omega i} - \boldsymbol{\Upsilon}_{\omega i}\right)}{\kappa_{\omega i}^2}\right], \end{aligned} \tag{24}$$

where $\boldsymbol{\Upsilon}_{vi} \in \Re^{12}$ and $\boldsymbol{\Upsilon}_{\omega i} \in \Re^{12}$ are the centers of the receptive filed, κ_{vi} and $\kappa_{\omega i}$ are the width of the Gaussian basis functions.

D. Graph Theory

The undirected graph always describes the connections among the multi-UAVs system. Given an undirected graph $\mathcal{G} = (\mathcal{V}, \mathcal{E}, \mathcal{A})$, it consists of nodes $\mathcal{V} = \{v_1, \ldots, v_n\}$ and the sets of edges $\mathcal{E} = \{(i, j),\ i, j \in \mathcal{V}, \text{and } i \neq j\}$, and $\mathcal{A} = [a_{ij}] \in \Re^{n\times n}$ denotes the weighted adjacency matrix of $\mathcal{G}$. If there exists an edge between node i and j, then $a_{ij} = a_{ji} \neq 0$ and otherwise $a_{ij} = a_{ji} = 0$. Moreover, a_{ii} equals to 0 for all $i \in \mathcal{V}$. The neighbors of node i is denoted by $\mathcal{N}_i = \{v_j :\ (v_j,\ v_i) \in \mathcal{E}\}$. The Laplacian matrix is defined by $\mathcal{L} = \mathcal{D} - \mathcal{A}$, where $\mathcal{D} = \mathrm{diag}\{d_1, \ldots, d_n\}$ with $d_i = \sum_{j=1}^{n} a_{ij}$. $\mathcal{G}$ is connected if there is a path from every node to each other node.

For leader-following multi-UAV system, the augmented graph $\bar{\mathcal{G}} \in (\bar{\mathcal{V}}, \bar{\mathcal{E}}, \bar{\mathcal{A}})$ for n UAVs including the leader is concerned. Let $\mathcal{H} = \mathrm{diag}\{h_1, \ldots, h_n\}$ denotes the leader adjacency matrix of the graph $\bar{\mathcal{G}}$. If the ith follower receives the information from the leader UAV, then $h_i > 0$ and otherwise $h_i = 0$.

Assumption 3: The topology of considered multi-UAV system is an undirected graph with at least one node having access to the leading node.

Lemma 1 [34]: For an undirected connected graph with the Laplacian matrix $\mathcal{L}$, if at least one $h_i > 0$, then symmetric matrix $\mathcal{L} + \mathcal{H}$ associated with $\bar{\mathcal{G}}$ is positive definite.

Remark 4: Assumption 3 and Lemma 1 preserve that the followers can receive the necessary information from the leader.

E. Control Objective

Given the reference comannds V_r and $\boldsymbol{\varphi}_r$ of V_i and $\boldsymbol{\varphi}_i$ respectively, the goal is to design the cooperative distributed event-triggered tracking controller such that

- All the closed-loop signals remain bounded and the synchronous speed and attitude tracking errors of each UAV are SGUUB in the presence of actuator faults, modeling uncertainties, and external disturbances.
- The signal transmission burden is considerably reduced for multi-UAV system. Also, the Zeno phenomenon is precluded such that the time between two consecutive switchings is lower bounded by a positive constant.

To achieve the control objective, the following assumption and lemmas are instrumental to stability analysis.

Assumption 4: The desired references V_r, $\boldsymbol{\varphi}_r$ and their time-derivatives up to second-order $\dot{V}_r$, $\ddot{\boldsymbol{\varphi}}_r$ are continuous and bounded.

Lemma 2 [35]: For any scalars $\varepsilon > 0$, $z \in \Re$, the following equation holds: $0 \leq |z| - \frac{z^2}{\sqrt{z^2+\varepsilon}} \leq \sqrt{\varepsilon}$.

Lemma 3 [36]: For any scalars $\varepsilon > 0$, $\vartheta \in \Re$, $0 \leq |\vartheta| - \vartheta\tanh(\frac{\vartheta}{\varepsilon}) \leq 0.2785\varepsilon$ holds.

III. Event-Triggered Adaptive Controller Design

A. Event-Triggering Mechanism

We are now at the position to provide the following triggering condition for translational and rotational kinematics, respectively.

1) Translational Kinematics:

$$\begin{aligned} & T_{xi0}(t) = \hat{T}_{xi0}\left(t_k^v\right), \quad \forall t \in \left[t_k^v, t_{k+1}^v\right) \\ & t_{k+1} = \inf\{t > t_k^v \,|\, |\hat{T}_{xi0}(t) - \hat{T}_{xi0}\left(t_k^v\right)| \geq a_1|\hat{T}_{xi0}\left(t_k^v\right)| + a_2\}, \end{aligned} \tag{25}$$

where $k = 0, 1, 2, \ldots, t_0 := 0$, $\hat{T}_{xi0}(t)$ is calculated by designed controller and will be presented in the following section, and $0 < a_1 < 1$, $a_2 > 0$ are design parameters.

In view of (25), it follows that $|\hat{T}_{xi0}(t) - \hat{T}_{xi0}(t_k^v)| \leq a_1|\hat{T}_{xi0}(t_k^v)| + a_2$ and $T_{xi0}(t) = \hat{T}_{xi0}(t_k^v)$ for all $t \in [t_k^v, t_{k+1}^v)$.

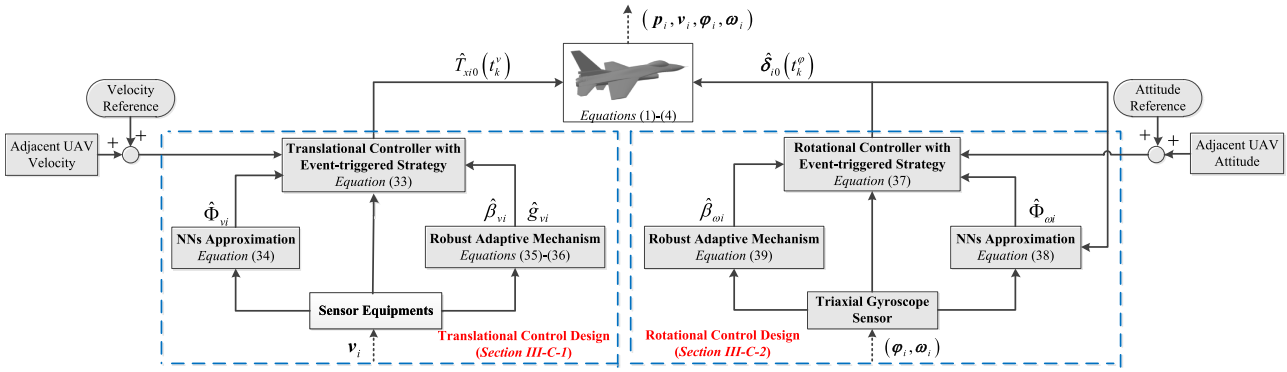

Fig. 3. Overall framework of the proposed control strategy.

TABLE I
STRUCTURAL AND AERODYNAMIC PARAMETER VALUES OF UAV

Coefficient	Value	Unit	Coefficient	Value	Unit
m_i	20.64	kg	b_i	1.96	m
S_i	1.37	m^2	$\bar{c}_i$	0.76	m
ρ	1.29	$\mathrm{kg}\cdot\mathrm{m}^{-3}$	g	9.8	$\mathrm{m}\cdot\mathrm{s}^{-2}$
J_{xxi}	1.607	$\mathrm{kg}\cdot\mathrm{m}^2$	J_{yyi}	7.51	$\mathrm{kg}\cdot\mathrm{m}^2$
J_{zzi}	7.18	$\mathrm{kg}\cdot\mathrm{m}^2$	J_{xzi}	0.59	$\mathrm{kg}\cdot\mathrm{m}^2$
c_{L0i}	0.1	/	$c_{L\alpha i}$	0.25	rad^{-1}
c_{D0i}	0.5	/	$c_{Y\beta i}$	−0.1	rad^{-1}
c_{l0i}	−0.001	/	$c_{l\beta i}$	−0.038	rad^{-1}
c_{lpi}	−0.213	$\mathrm{rad}^{-1}\cdot\mathrm{s}$	c_{lri}	0.114	$\mathrm{rad}^{-1}\cdot\mathrm{s}$
$c_{l\delta ai}$	−0.056	rad^{-1}	$c_{l\delta ri}$	0.014	rad^{-1}
c_{m0i}	0.022	/	$c_{m\alpha i}$	−0.473	rad^{-1}
c_{mqi}	−3.449	$\mathrm{rad}^{-1}\cdot\mathrm{s}$	$c_{m\delta ei}$	−0.364	rad^{-1}
c_{n0i}	0.022	/	$c_{n\beta i}$	0.036	rad^{-1}
c_{npi}	−0.151	$\mathrm{rad}^{-1}\cdot\mathrm{s}$	c_{nri}	−0.195	$\mathrm{rad}^{-1}\cdot\mathrm{s}$
$c_{n\delta ai}$	−0.036	rad^{-1}	$c_{n\delta ri}$	−0.055	rad^{-1}

Since $t_0 := 0$, these results hold for each $k = 1, 2, 3\ldots$, and there exists

$$|\hat{T}_{xi0}(t) - T_{xi0}(t)| \le a_1 |T_{xi0}(t)| + a_2, \quad \forall t \ge 0. \tag{26}$$

Define $p_1(t) = \frac{\hat{T}_{xi0}(t) - T_{xi0}(t)}{a_1|T_{xi0}(t)| + a_2}$. It follows that $|p_1(t)| \le 1$. This fact implies the following inequality for all time:

$$\hat{T}_{xi0}(t) - T_{xi0}(t) = a_1 p_1(t) T_{xi0}(t) + a_2 p_1(t). \tag{27}$$

Using (27) yields

$$T_{xi0} = \frac{\hat{T}_{xi0}}{1 + a_1 p_1} - \frac{a_2 p_1}{1 + a_1 p_1}. \tag{28}$$

2) Rotational Kinematics:

$$\begin{aligned}
&\boldsymbol{\delta}_{i0}(t) = \hat{\boldsymbol{\delta}}_{i0}\left(t_k^\varphi\right), \quad \forall t \in \left[t_k^\varphi, t_{k+1}^\varphi\right), \\
&t_{k+1}^\varphi = \inf\{t > t_k^\varphi \,|\, |\hat{\delta}_{ai0}(t) - \hat{\delta}_{ai0}(t_k^\varphi)| \ge b_1 |\hat{\delta}_{ai0}(t_k^\varphi)| + b_2 \\
&\qquad \text{or} |\hat{\delta}_{ei0}(t) - \hat{\delta}_{ei0}(t_k^\varphi)| \ge b_1 |\hat{\delta}_{ei0}(t_k^\varphi)| + b_2 \\
&\qquad \text{or} |\hat{\delta}_{ri0}(t) - \hat{\delta}_{ri0}(t_k^\varphi)| \ge b_1 |\hat{\delta}_{ri0}(t_k^\varphi)| + b_2\}
\end{aligned} \tag{29}$$

where $\hat{\boldsymbol{\delta}}_{i0}(t) = [\hat{\delta}_{ai0}(t), \hat{\delta}_{ei0}(t), \hat{\delta}_{ri0}(t)]^{\mathrm{T}}$ is produced by designed controller and will be described in the following section, and $0 < b_1 < 1$, $b_2 > 0$ are design parameters.

Similarly, we define $p_2(t) = \frac{\hat{\delta}_{ai0}(t) - \delta_{ai0}(t)}{b_1|\delta_{ai0}(t)| + b_2}$, $p_3(t) = \frac{\hat{\delta}_{ei0}(t) - \delta_{ei0}(t)}{b_1|\delta_{ei0}(t)| + b_2}$, $p_4(t) = \frac{\hat{\delta}_{ri0}(t) - \delta_{ri0}(t)}{b_1|\delta_{ri0}(t)| + b_2}$. Then we arrive at

$$\boldsymbol{\delta}_{i0} = \boldsymbol{D}_i \hat{\boldsymbol{\delta}}_{i0} + \boldsymbol{\sigma}_i, \tag{30}$$

where $\boldsymbol{D}_i = \mathrm{diag}\{D_{i1}, D_{i2}, D_{i3}\}$ and $\boldsymbol{\sigma}_i = [\sigma_{i1}, \sigma_{i2}, \sigma_{i3}]^{\mathrm{T}}$ with

$$D_{ij} = \frac{1}{1 + b_1 p_{j+1} \mathrm{sign}(\delta_{i0j})}, \sigma_{ij} = \frac{-b_2 p_{j+1}}{1 + b_1 p_{j+1} \mathrm{sign}(\delta_{i0j})}.$$

Remark 5: Differently from existing works [23], [24], the event-triggered mechanisms are first introduced in thrust T_{xi0} and control surface $\boldsymbol{\delta}_{i0}$ to obtain $\hat{T}_{xi0}$ and $\hat{\boldsymbol{\delta}}_{i0}$. This operation ensures that the time instants of updating control signals are determined by event-triggering mechanism instead of traditional periodical updating, which significantly reduces the signal transmission frequency, while saving on system resources.

B. Error Transformations

1) Translational Kinematics: Based on speed tracking errors $\tilde{V}_i = V_i - V_r$ and $\tilde{V}_j = V_j - V_r$, the objective of guaranteeing speed synchronization tracking is equivalent to make $\tilde{V}_i' \to 0$.

$$\tilde{V}_i' = \lambda_{i1} \tilde{V}_i + \lambda_{i2} \sum_{j \in \mathcal{N}_i} a_{ij} (\tilde{V}_i - \tilde{V}_j), \tag{31}$$

where λ_{i1} and λ_{i2} are positive design parameters.

2) Rotational Kinematics: Similarly, the attitude synchronization tracking error is expressed as

$$\boldsymbol{e}_{\varphi i}' = \lambda_{i3} \boldsymbol{e}_{\varphi i} + \lambda_{i4} \sum_{j \in \mathcal{N}_i} a_{ij} (\boldsymbol{e}_{\varphi i} - \boldsymbol{e}_{\varphi j}), \tag{32}$$

where $\boldsymbol{e}_{\varphi i} = \boldsymbol{\varphi}_i - \boldsymbol{\varphi}_r$, $\boldsymbol{e}_{\varphi j} = \boldsymbol{\varphi}_j - \boldsymbol{\varphi}_r$, and $\lambda_{i3}, \lambda_{i4}$ are positive design parameters.

C. Controller Design

Following the double-layer control structure, the translational and rotational control design are proposed independently. Specifically, $\hat{T}_{xi0}$ and $\hat{\boldsymbol{\delta}}_{i0}$ designs are given. To facilitate readers comprehension, the overall block diagram of the proposed control scheme is presented in Fig. 3.

TABLE II
INITIAL STATES OF UAVS

	$x_i\,(0)$	$y_i\,(0)$	$z_i\,(0)$	$V_i\,(0)$	$\phi_i\,(0)$	$\theta_i\,(0)$	$\psi_i\,(0)$	$p_i\,(0)$	$q_i\,(0)$	$r_i\,(0)$
Leader	-20m	20m	100m	40m/s	0°	1°	0°	0rad/s	0rad/s	0rad/s
Follower 1	0m	0m	100m	40.5m/s	0°	1°	0°	0rad/s	0rad/s	0rad/s
Follower 2	-40m	40m	100m	40m/s	0°	1°	0°	0rad/s	0rad/s	0rad/s

TABLE III
CONTROLLER PARAMETERS

Coefficient	Value	Coefficient	Value	Coefficient	Value	Coefficient	Value
c_{v1}, c_{v2}, c_{v3}	10	a_2	$0.5\,(t \le 14)$	$\boldsymbol{K}_{11}, \boldsymbol{K}_{12}, \boldsymbol{K}_{13}$	$\mathrm{diag}\,\{50, 50, 51\}\,(t \le 5)$	$\boldsymbol{K}_{21}, \boldsymbol{K}_{22}, \boldsymbol{K}_{23}$	$\mathrm{diag}\,\{50, 50, 51\}\,(t \le 5)$
$\varepsilon_{v1}, \varepsilon_{v2}, \varepsilon_{v3}$	0.1		$1\,(t > 14)$		$\mathrm{diag}\,\{45, 45, 45\}\,(5 < t \le 15)$		$\mathrm{diag}\,\{45, 45, 46\}\,(5 < t \le 15)$
$\varepsilon_{\omega 1}, \varepsilon_{\omega 2}, \varepsilon_{\omega 3}$	1	b_1	0.01		$\mathrm{diag}\,\{40, 40, 40\}\,(t > 15)$		$\mathrm{diag}\,\{40, 40, 40\}\,(t > 15)$
a_1	0.01	b_2	1	$\gamma_{\omega i1}, \gamma_{\omega i2}$	0.01	$\sigma_{\omega i1}, \sigma_{\omega i2}$	25

1) Translational Kinematics: To achieve the control objective in Section II-D, we employ the following dynamic controller $\hat{T}_{xi0}$:

$$\hat{T}_{xi0} = \frac{-\left(1 + a_1\right) B_{vi}}{\zeta_{vi}}, \tag{33}$$

where $\zeta_{vi} = \frac{u_i \lambda_i}{m_i V_i}$ with $\lambda_i = \lambda_{i1} + \lambda_{i2} \sum_{j \in \mathcal{N}_i} a_{ij}$, and B_{vi} is defined as

$$B_{vi} = (\alpha_{vi} - r_{vi}) \hat{\beta}_{vi} \tanh\left(\frac{\tilde{V}_i'(\alpha_{vi} - r_{vi})\hat{\beta}_{vi}}{\varepsilon_{vi}}\right) + \hat{g}_{vi}\zeta_{vi} \tanh\left(\frac{\tilde{V}_i' \hat{g}_{vi}\zeta_{vi}}{\varepsilon_{vi}}\right),$$

where $\alpha_{vi} = c_{vi}\tilde{V}_i' + \lambda_i\left(\frac{\boldsymbol{v}_i^{\mathrm{T}}}{V_i}\left(\boldsymbol{R}_1^{\mathrm{T}}\boldsymbol{g} + \frac{\boldsymbol{F}_{i0}}{m_i}\right) + \frac{\hat{\Phi}_{vi}\boldsymbol{v}_i^{\mathrm{T}}\boldsymbol{\Xi}_{vi}}{2h_{vi1}^2 V_i} + \frac{\boldsymbol{v}_i^{\mathrm{T}}\boldsymbol{v}_i\tilde{V}_i'}{2h_{vi2}^2 V_i^2}\right)$ with $\boldsymbol{\Xi}_{vi} = \left[\frac{\tilde{V}_i' v_{i1}\boldsymbol{\varsigma}_{vi1}^{\mathrm{T}}\boldsymbol{\varsigma}_{vi1}}{V_i}, \frac{\tilde{V}_i' v_{i2}\boldsymbol{\varsigma}_{vi2}^{\mathrm{T}}\boldsymbol{\varsigma}_{vi2}}{V_i}, \frac{\tilde{V}_i' v_{i3}\boldsymbol{\varsigma}_{vi3}^{\mathrm{T}}\boldsymbol{\varsigma}_{vi3}}{V_i}\right]^{\mathrm{T}}$ and $r_{vi} = \lambda_i \dot{V}_r + \lambda_{i2}\sum_{j \in \mathcal{N}_i} a_{ij}\dot{\tilde{V}}_j$. The adaptive parameters $\hat{\Phi}_{vi}$, $\hat{g}_{vi}$ and $\hat{\beta}_{vi}$ are updated by

$$\dot{\hat{\Phi}}_{vi} = \lambda_i \frac{\gamma_{vi1}\tilde{V}_i'\boldsymbol{v}_i^{\mathrm{T}}\boldsymbol{\Xi}_{vi}}{2h_{vi1}^2 V_i} - \sigma_{vi1}\hat{\Phi}_{vi}, \tag{34}$$

$$\dot{\hat{g}}_{vi} = \gamma_{vi2}|\tilde{V}_i'|\zeta_{vi} - \sigma_{vi2}\hat{g}_{vi}, \tag{35}$$

$$\dot{\hat{\beta}}_{vi} = \gamma_{vi3}\tilde{V}_i'\left(\alpha_{vi} - r_{vi}\right) - \sigma_{vi3}\hat{\beta}_{vi}, \tag{36}$$

where $h_{vi1}, h_{vi2}, \gamma_{vi1}, \gamma_{vi2}, \gamma_{vi3}, \sigma_{vi1}, \sigma_{vi2}, \sigma_{vi3}, \varepsilon_{vi}$ are positive design parameters.

Theorem 1: Consider the translational kinematics (15) composed by the adaptive tracking controller (33) and parameter adaptation laws (34)-(36). Let Assumptions 3-4 hold. There exist adjustable parameters $\lambda_{i1}, \lambda_{i2}, c_{vi}, \varepsilon_{vi}, h_{vi1}, h_{vi2}, \gamma_{vij}$ and σ_{vij} $(i = 1, 2, \ldots, N, j = 1, 2, 3)$ such that:

1) All signals of the translational subsystem are SGUUB in the presence of actuator faults, modeling uncertainties, and external disturbances.

2) Speed synchronization tracking error $\tilde{V}_i'$ is such that $\lim_{t\to\infty}|\tilde{V}_i'| \le \mu_{Vi}$ with $\mu_{Vi} > 0$ a constant.

3) The signal transmission burden for translational subsystem is considerably reduced. Meanwhile the Zeno phenomenon is precluded.

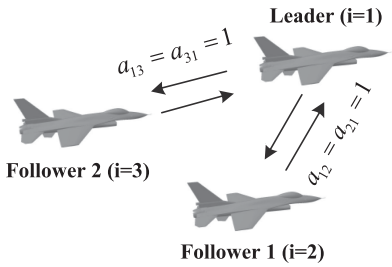

Fig. 4. Communication topology.

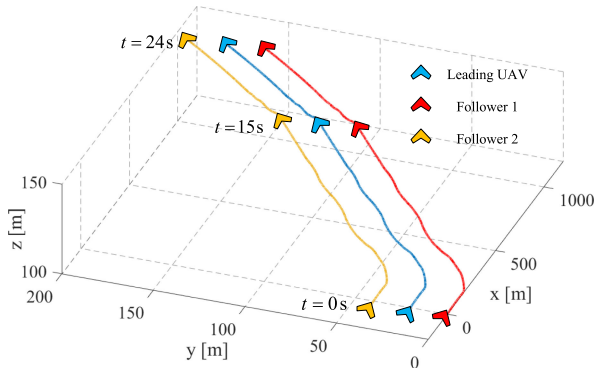

Fig. 5. Trajectories of UAV formation.

We have the above convergence result. The proof is given in Appendix A.

2) Rotational Kinematics: To obtain the control objective in Section II-D, we propose the dynamic controller $\hat{\boldsymbol{\delta}}_{i0}$ as follows:

$$\hat{\boldsymbol{\delta}}_{i0} = -\left(\boldsymbol{J}_{i0}^{-1}\boldsymbol{C}_{i0}\right)^{\mathrm{T}} \frac{\boldsymbol{e}_{\omega i}\hat{\beta}_{\omega i}^2\boldsymbol{\zeta}_{\omega i}^{\mathrm{T}}\boldsymbol{\zeta}_{\omega i}}{\sqrt{\hat{\beta}_{\omega i}^2\boldsymbol{e}_{\omega i}^{\mathrm{T}}\boldsymbol{e}_{\omega i}\boldsymbol{\zeta}_{\omega i}^{\mathrm{T}}\boldsymbol{\zeta}_{\omega i} + \varepsilon_{\omega i}}}, \tag{37}$$

where $\boldsymbol{\zeta}_{\omega i} = \boldsymbol{K}_{2i}\boldsymbol{e}_{\omega i} + \boldsymbol{J}_{i0}^{-1}\boldsymbol{S}(\boldsymbol{J}_{i0}\boldsymbol{\omega}_i) + \boldsymbol{J}_{i0}^{-1}\boldsymbol{N}_{i0} + \frac{\hat{\Phi}_{\omega i}\boldsymbol{\Xi}_{\omega i}}{2h_{\omega i1}^2} + \frac{\boldsymbol{e}_{\omega i}}{2h_{\omega i2}^2} + \lambda_i'(\boldsymbol{R}_2^{-1})^{\mathrm{T}}\boldsymbol{e}_{\varphi i}' - \dot{\boldsymbol{\omega}}_{di}$ with $\lambda_i' = \lambda_{i3} + \lambda_{i4}\sum_{j \in \mathcal{N}_i} a_{ij}$ and $\boldsymbol{\Xi}_{\omega i} = [e_{\omega i1}\boldsymbol{\varsigma}_{\omega i1}^{\mathrm{T}}\boldsymbol{\varsigma}_{\omega i1}, e_{\omega i2}\boldsymbol{\varsigma}_{\omega i2}^{\mathrm{T}}\boldsymbol{\varsigma}_{\omega i2}, e_{\omega i3}\boldsymbol{\varsigma}_{\omega i3}^{\mathrm{T}}\boldsymbol{\varsigma}_{\omega i3}]^{\mathrm{T}}$. The adaptive parameters $\hat{\Phi}_{\omega i}$ and $\hat{\beta}_{\omega i}$ are proposed as

$$\dot{\hat{\Phi}}_{\omega i} = \gamma_{\omega i1}\frac{\boldsymbol{e}_{\omega i}^{\mathrm{T}}\boldsymbol{\Xi}_{\omega i}}{2h_{\omega i1}^2} - \sigma_{\omega i1}\hat{\Phi}_{\omega i}, \tag{38}$$

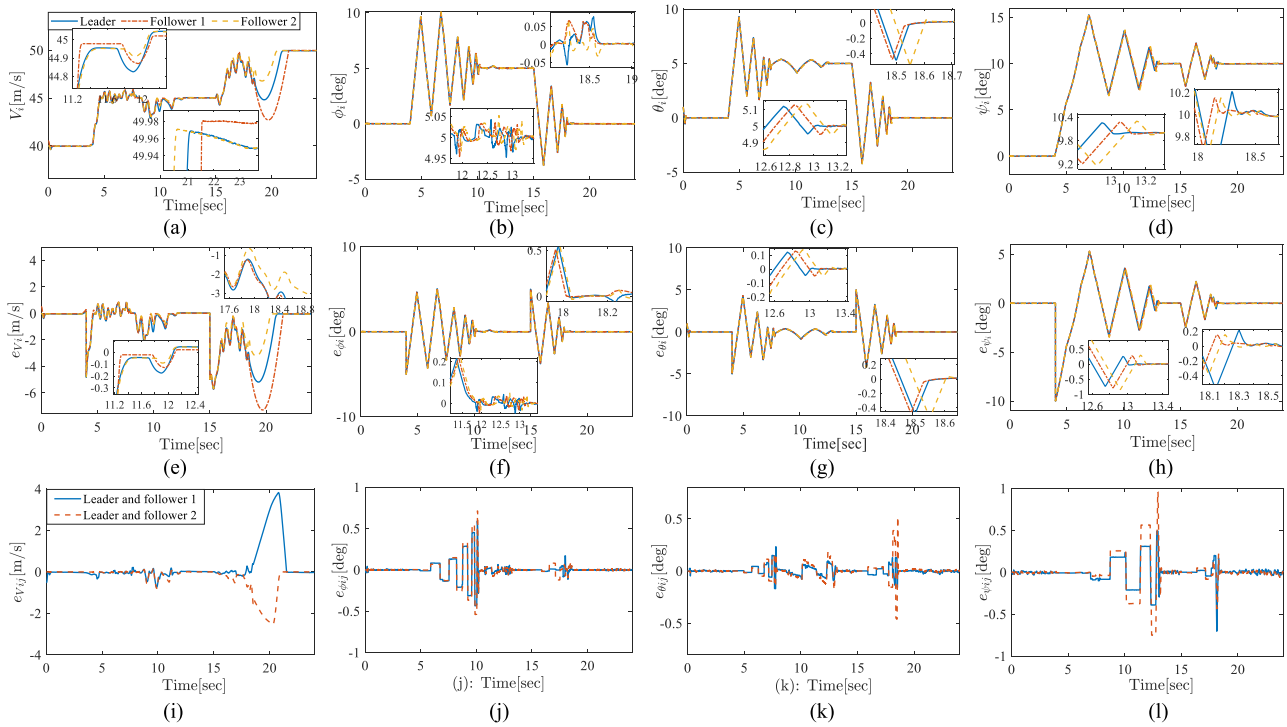

Fig. 6. Speed and attitude angle tracking results and errors by using proposed controller. (a)-(l) show the curves of state responses and errors. (a) Speed response (b) Roll angle response (c) Pitch angle response (d) Yaw angle response (e) Tracking error of speed (f) Tracking error of roll angle (g) Tracking error of pitch angle (h) Tracking error of yaw angle (i) Synchronization error of speed (j) Synchronization error of roll angle (k) Synchronization error of pitch angle (l) Synchronization error of yaw angle.

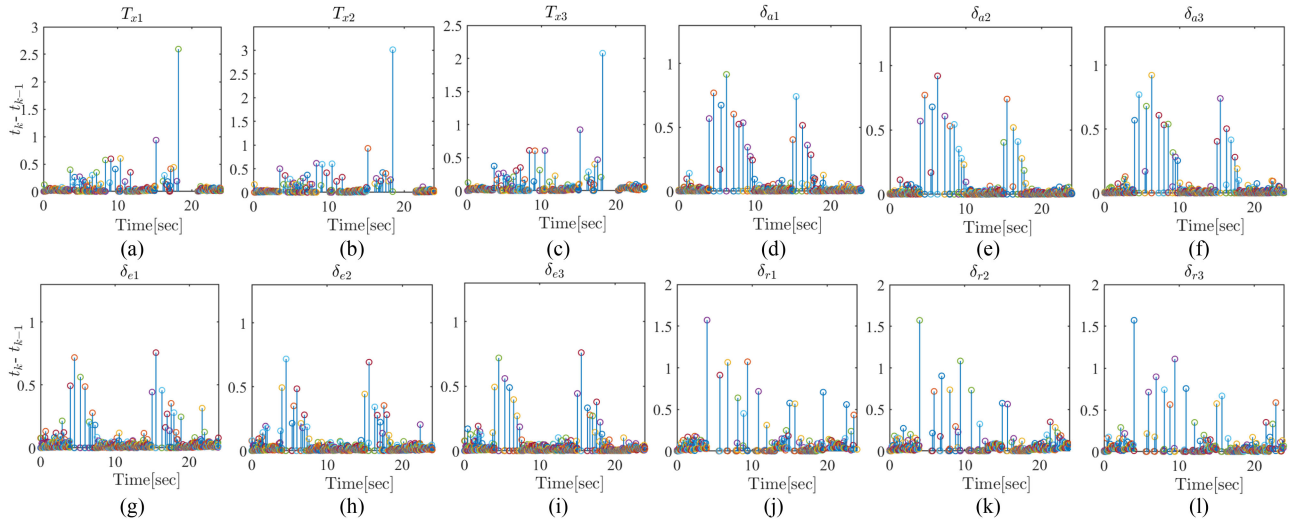

Fig. 7. Time interval of triggering events. (a)-(l) show the curves of triggering time intervals. (a) Control signal T_{x1} (b) Control signal T_{x2} (c) Control signal T_{x3} (d) Control signal δ_{a1} (e) Control signal δ_{a2} (f) Control signal δ_{a3} (g) Control signal δ_{e1} (h) Control signal δ_{e2} (i) Control signal δ_{e3} (j) Control signal δ_{r1} (k) Control signal δ_{r2} (l) Control signal δ_{r3}.

$$\dot{\hat{\beta}}_{\omega i} = \gamma_{\omega i2} \boldsymbol{e}_{\omega i}^{\mathrm{T}} \boldsymbol{\zeta}_{\omega i} - \sigma_{\omega i2} \hat{\beta}_{\omega i}. \tag{39}$$

where $h_{\omega i1}$, $h_{\omega i2}$, $\gamma_{\omega i1}$, $\gamma_{\omega i2}$, $\sigma_{\omega i1}$, $\sigma_{\omega i2}$, $\varepsilon_{\omega i}$ are positive design parameters.

Theorem 2: Consider the rotational kinematics (16), (22) composed by the adaptive tracking controller (37) and parameter adaptation laws (38)-(39). Let Assumptions 1-4 hold. There exist adjustable parameters λ_{i3}, λ_{i4}, $\boldsymbol{K}_{ji}$, $\varepsilon_{\omega i}$, $h_{\omega ij}$, $\gamma_{\omega ij}$ and $\sigma_{\omega ij}$ $(i = 1, 2, \ldots, N, j = 1, 2)$ such that:

1) All signals of the rotational subsystem are SGUUB in the presence of actuator faults, modeling uncertainties, and external disturbances.

2) Attitude synchronization tracking error $\boldsymbol{e}'_{\varphi i}$ is such that $\lim_{t\to\infty} \|\boldsymbol{e}'_{\varphi i}\| \leq \mu_{\varphi i}$ with $\mu_{\varphi i} > 0$ a constant.

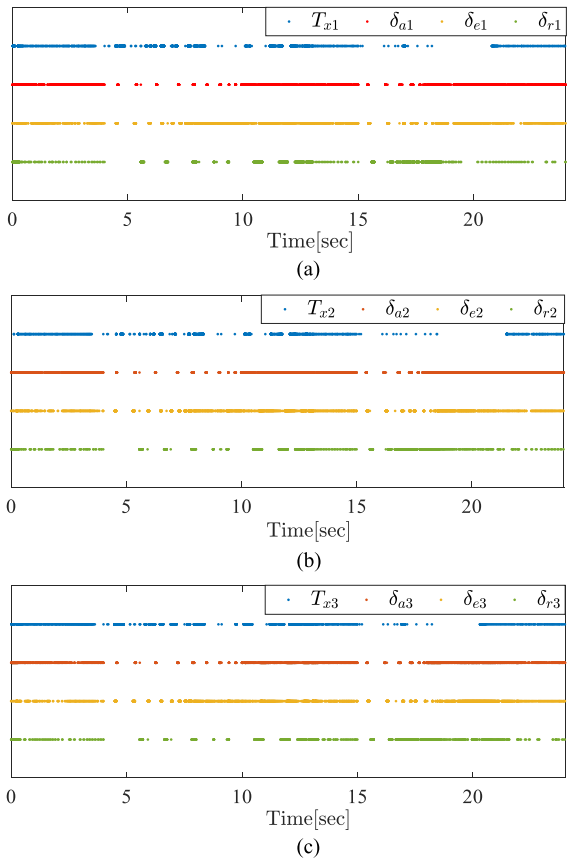

Fig. 8. Triggering time of control signals. (a)-(c) show the curves of triggering event. (a) Leading UAV (b) Follower 1 (c) Follower 2.

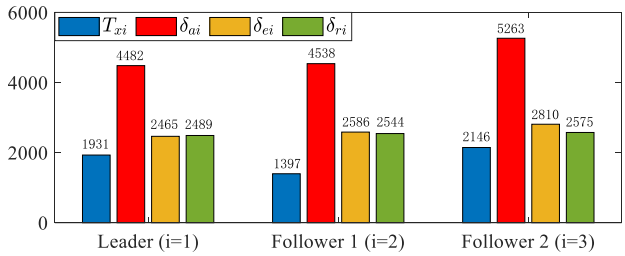

Fig. 9. Number of times for control transmission.

3) The signal transmission burden for rotational subsystem is considerably reduced. Meanwhile the Zeno phenomenon is avoided.

Now the corresponding proof is given in Appendix B.

In Theorems 1 and 2, we have designed the controllers that guarantee event-triggered convergence and fault-tolerance for speed and attitude synchronization tracking simultaneously under model uncertainties, external disturbances and actuator faults. The proposed controllers have the following features in comparison with the related existing controllers.

• Differently from control schemes for single six-DOF fixed-wing UAV of [23], [24] with no consideration of fault-tolerant and event-triggered strategy, our scheme extends design to event-triggered adaptive fault-tolerant control scheme for multiple six-DOF fixed-wing UAVs.

• The modeling uncertainties are effectively handled with the help of neural network approximations for $\boldsymbol{\Delta}_{vi}$ and $\boldsymbol{\Delta}'_{\omega i}$. Meanwhile, to deal with the actuator faults, the bound estimations for parameters $\beta_{vi} = 1/\rho_{Ti}$, $g_{vi} = \beta_{vi} \sup_{t\geq 0} T_{xif}$ in translational control protocol, and $\beta_{\omega i} = 1/g_{\omega i}$, $g_{\omega i} = \inf_{t\geq 0} \lambda_{\min}(\boldsymbol{J}_{i0}^{-1}\boldsymbol{C}_0(\boldsymbol{\delta}_i)\boldsymbol{\rho}_{\delta i}\boldsymbol{D}_i(\boldsymbol{J}_{i0}^{-1}\boldsymbol{C}_0(\boldsymbol{\delta}_i))^{\mathrm{T}})$ in rotational control design are introduced in (35), (36) and (39). Further, we employ the features of the smooth function $\vartheta \tanh(\frac{\vartheta}{\varepsilon})$ in design of $\hat{T}_{xi0}$ in (33), and function $\frac{z^2}{\sqrt{z^2+\varepsilon}}$ when designing $\hat{\boldsymbol{\delta}}_{i0}$ in (37).

IV. Simulation Results and Analysis

A. Simulation Scenario

In order to illustrate the effectiveness and superiority of the proposed event-triggered adaptive control scheme, several representative simulations are conducted in this section. The structure parameters and coefficient values are referred to [23] and listed in Table I . Three networked fixed-wing UAVs are considered to complete the mission of coordinated turn and climb. The initial conditions are given in Table II . The corresponding communication topology is illustrated in Fig. 4. The reference commands are set as

$$V_r = \begin{cases} 40m/\mathrm{s}, & 0\mathrm{s} \leq t \leq 4\mathrm{s} \\ 45m/\mathrm{s}, & 4\mathrm{s} < t \leq 15\mathrm{s} \\ 50m/\mathrm{s}, & 15\mathrm{s} < t \leq 24\mathrm{s} \end{cases},$$

$$[\phi_r, \theta_r, \psi_r]^{\mathrm{T}} = \begin{cases} [0\,\mathrm{deg}, 0\,\mathrm{deg}, 0\,\mathrm{deg}]^{\mathrm{T}}, & 0\mathrm{s} \leq t \leq 4\mathrm{s} \\ [5\,\mathrm{deg}, 5\,\mathrm{deg}, 10\,\mathrm{deg}]^{\mathrm{T}}, & 4\mathrm{s} < t \leq 15\mathrm{s} \\ [0\,\mathrm{deg}, 0\,\mathrm{deg}, 10\,\mathrm{deg}]^{\mathrm{T}}, & 15\mathrm{s} < t \leq 24\mathrm{s} \end{cases}.$$

During the flight, suppose that the external disturbances in speed and attitude motion are described as $\boldsymbol{d}_{vi} = [0.1\sin(\pi t), 0.1\sin(4t), 0.1\cos(\pi t)]^{\mathrm{T}}$ and $\boldsymbol{d}_{\omega i} = [0.2\cos(\pi t), 0.1\sin(\pi t), 0.2\sin(\pi t)]^{\mathrm{T}}$ $(i = 1, 2, 3)$; Meanwhile, the rudder of follower 2 loses its effectiveness described by $\boldsymbol{\rho}_{\delta 3} = \mathrm{diag}\{1, 1, 0.9\}$ during $t \in (19, 22]$s, while the leader and follower 1 are healthy during flight. The main parameters of the proposed control scheme are set in Table III .

B. Results and Analyses

Scenario 1: In the first scenario, the simulation is conducted by applying the proposed event-triggered adaptive control scheme to the multi-UAV dynamic models in above simulation scenario. Fig. 5 depicts the flight trajectories of UAV formation, from which we can observe that the coordinated turn and climb with satisfactory speed and attitude synchronization tracking is achieved. The detailed speed and attitude tracking performances are shown in Fig. 6. From Fig. 6(a)-(d), it can be observed that speed and attitude both converge availably to the desired trajectories, which validates the effectiveness of proposed schemes. Additionally, the tracking errors of speed and attitude are depicted in Fig. 6(e)-(h). From Fig. 6(i)-(l), we see that the proposed scheme can guarantee the synchronization tracking of speed and attitude for UAVs. With the proposed control scheme, the time intervals of each event for UAVs are presented

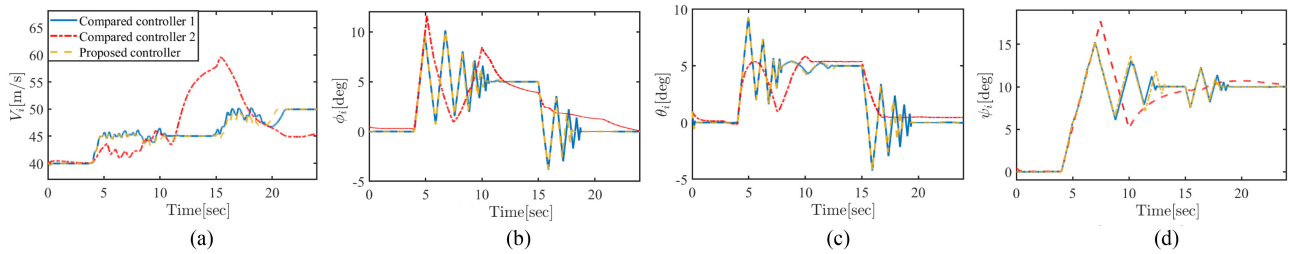

Fig. 10. Control performance comparison of speed and attitude tracking under two comparative controllers and proposed controller (taking the follower 2 for example). (a)-(d) show the curves of state responses. (a) Speed response (b) Roll angle response (c) Pitch angle response (d) Yaw angle response.

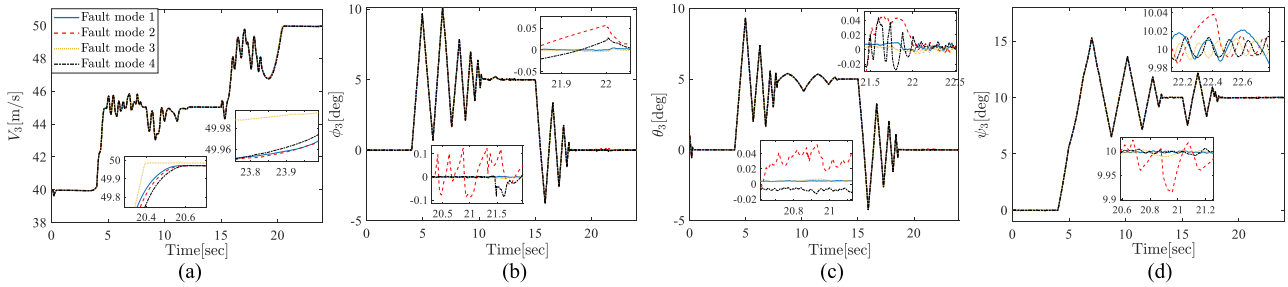

Fig. 11. Speed and attitude tracking of follower 2 under different fault modes. (a)-(d) show the curves of state responses. (a) Speed response (b) Roll angle response (c) Pitch angle response (d) Yaw angle response.

in Fig. 7(a)-(l) and meanwhile Fig. 8(a)-(c) list the time at which the events are triggered. Then, the numbers of events triggered of control inputs for each UAV during 24 s are calculated, as shown in Fig. 9.

Scenario 2: To illustrate the superiority of proposed control scheme, two comparative control methods are conducted. The first comparative method is obtained by removing the event-triggered strategy from our proposed control scheme, which is used to show that the event-triggered feature reduces the control transmission burden, and meanwhile maintains the control performances (denoted as "Compared controller 1" hereafter). Moreover, we find the control approach designed in [22] (regarded as "Compared controller 2" hereafter) worth for comparison because it deals with the flight control for six-DOF fixed-wing UAV as well, however without fault-tolerant and event-triggered control. As a consequence, the comparative simulation results are depicted in Fig. 10 (taking the follower 2 for example), which shows the tracking curves of speed and attitude under the three control schemes. Obviously, the compared controller 2 breaks down in speed and attitude tracking when reacts to the external disturbances and actuator faults, which obtains the worst performance of three control schemes. In addition, the integral absolute error (IAE) and control transmission times are utilized here as performance indices. The results are summarized in Tables IV and V . It is explicit that the proposed scheme saves 86.67% of control transmission burden, and meanwhile maintains the good control performances compared to two comparative controllers.

TABLE IV
IAE ASSESSMENT OF TRACKING PERFORMANCE FOR SCENARIO 2

Control Schemes	V_3	ϕ_3	θ_3	ψ_3
Compared controller 1	15.8	18	14.3	25
Compared controller 2	88.5	33.1	19.2	37.4
Proposed controller	17.8	16.4	13.4	25.6

TABLE V
CONTROL TRANSMISSION TIMES FOR SCENARIO 2

Control Schemes	T_{x3}	δ_{a3}	δ_{e3}	δ_{r3}
Compared controller 1	24000	24000	24000	24000
Compared controller 2	24000	24000	24000	24000
Proposed controller	2146	5263	2810	2575

Scenario 3: To further evaluate the sensitivity of proposed event-triggered conditions, we consider the following four different fault modes:

Fault mode 1: The rudder of follower 2 loses its effectiveness described by $\boldsymbol{\rho}_{\delta_3} = \mathrm{diag}\{1, 1, 0.9\}$ during $t \in (19, 22]$s.

Fault mode 2: Based on the fault mode 1, the rudder of follower 2 also suffers from the bias fault introduced as $\boldsymbol{\delta}_{3f} = [0, 0, 1]^{\mathrm{T}}$ during $t \in (19, 22]$s.

Fault mode 3: The elevator of follower 2 loses its effectiveness also with the bias fault described by $\boldsymbol{\rho}_{\delta_3} = \mathrm{diag}\{0.9, 1, 1\}$ and $\boldsymbol{\delta}_{3f} = [0.5, 0, 0]^{\mathrm{T}}$ during $t \in (19, 22]$s.

Fault mode 4: The aileron of follower 2 loses its effectiveness described by $\boldsymbol{\rho}_{\delta_3} = \mathrm{diag}\{1, 0.9, 1\}$ and meanwhile suffers from the bias fault as $\boldsymbol{\delta}_{3f} = [0, 1, 0]^{\mathrm{T}}$ during $t \in (19, 22]$s.

Based on above fault modes, the fault-tolerant performances of follower 2 for different fault modes are shown in Fig. 11. Desired robustness with proposed controller is demonstrated in case of above four fault modes in Fig. 11. From Fig. 11, we can notice that the fault-tolerant property guarantees the stable tracking of speed and attitude for follower 2 in the presence of different faults on three control surfaces.

V. Conclusion

An event-triggered cooperative synchronization fault-tolerant control methodology has been designed for multiple UAVs subject to actuator faults, modeling uncertainties, and external disturbances. As compared with most existing works concerning two-degree or only attitude/longitudinal dynamics, six-DOF dynamics with twelf-state-variables has been considered. Specifically, event-triggering mechanisms are introduced into translational and rotational subsystems independently, which reduces the signal transmission burden, while saving on system resources. The actuator faults as well as the network induced errors are dealt with by the bound estimation approach and some well-defined smooth functions. All closed-loop signals are SGUUB and meanwhile the synchronization tracking of speed and attitude for UAVs is achieved well. We note that the extension of event-triggering mechanism to communication between UAVs is open. Also, involving output/state constrains and prescribed performances into our proposed scheme remains a good point for future research.

Appendix A
Proof of Theorem 1

Noting (15) and (31), we obtain the derivative of $\tilde{V}_i'$ as

$$\dot{\tilde{V}}_i' = \lambda_i \left[\frac{\boldsymbol{v}_i^{\mathrm{T}}}{V_i} \left(\boldsymbol{R}_1^{\mathrm{T}} \boldsymbol{g} + \frac{\boldsymbol{F}_{i0}}{m_i} \right) + \frac{\boldsymbol{v}_i^{\mathrm{T}}}{V_i} (\boldsymbol{\Delta}_{vi} + \boldsymbol{d}_{vi}) \right] + \lambda_i \frac{u_i \rho_{Ti} T_{xi0}}{m_i V_i} + \lambda_i \frac{u_i T_{xif}}{m_i V_i} - \lambda_i \dot{V}_r - \lambda_{i2} \sum_{j \in \mathcal{N}_i} a_{ij} \dot{\tilde{V}}_j, \tag{A1}$$

Substituting (28) into (A1) gives

$$\dot{\tilde{V}}_i' = \lambda_i \left[\frac{\boldsymbol{v}_i^{\mathrm{T}}}{V_i} \left(\boldsymbol{R}_1^{\mathrm{T}} \boldsymbol{g} + \frac{\boldsymbol{F}_{i0}}{m_i} \right) + \frac{\boldsymbol{v}_i^{\mathrm{T}}}{V_i} (\boldsymbol{\Delta}_{vi} + \boldsymbol{d}_{vi}) \right] + \frac{\zeta_{vi} \rho_{Ti} \hat{T}_{xi0}}{1 + a_1 p_1} + \zeta_{vi} \varpi_{vi} - r_{vi}, \tag{A2}$$

where $\varpi_{vi} = T_{xif} - \frac{a_2 p_1 \rho_{Ti}}{1 + a_1 p_1}$.

Integrating (23) leads to

$$\boldsymbol{v}_i^{\mathrm{T}} (\boldsymbol{\Delta}_{vi} + \boldsymbol{d}_{vi}) = \boldsymbol{v}_i^{\mathrm{T}} \begin{bmatrix} \boldsymbol{W}_{vi1}^{*\mathrm{T}} \boldsymbol{\varsigma}_{vi1} + \tau_{vi1} + d_{vi1} \\ \boldsymbol{W}_{vi2}^{*\mathrm{T}} \boldsymbol{\varsigma}_{vi2} + \tau_{vi2} + d_{vi2} \\ \boldsymbol{W}_{vi3}^{*\mathrm{T}} \boldsymbol{\varsigma}_{vi3} + \tau_{vi3} + d_{vi3} \end{bmatrix} = \sum_{j=1}^{3} v_{ij} \boldsymbol{W}_{vij}^{*\mathrm{T}} \boldsymbol{\varsigma}_{vij} + \sum_{j=1}^{3} v_{ij} (\tau_{vij} + d_{vij}), \tag{A3}$$

where $\boldsymbol{v}_i = [v_{i1}, v_{i2}, v_{i3}]^{\mathrm{T}} = [u_i, v_i, w_i]^{\mathrm{T}}$.

Using Young's inequality, we arrive at

$$\frac{\tilde{V}_i'}{V_i} v_{ij} \boldsymbol{W}_{vij}^{*\mathrm{T}} \boldsymbol{\varsigma}_{vij} \le \frac{\tilde{V}_i'^2 v_{ij}^2 \Phi_{vi} \boldsymbol{\varsigma}_{vij}^{\mathrm{T}} \boldsymbol{\varsigma}_{vij}}{2 h_{vi1}^2 V_i^2} + \frac{h_{vi1}^2}{2},$$

$$\frac{\tilde{V}_i'}{V_i} v_{ij} (\tau_{vij} + d_{vij}) \le \frac{\tilde{V}_i'^2 v_{ij}^2}{2 h_{vi2}^2 V_i^2} + \frac{h_{vi2}^2 \bar{\tau}_{vij}^2}{2}, \tag{A4}$$

where $\Phi_{vi} = \max\{\boldsymbol{W}_{vi1}^{*\mathrm{T}} \boldsymbol{W}_{vi1}^*, \boldsymbol{W}_{vi2}^{*\mathrm{T}} \boldsymbol{W}_{vi2}^*, \boldsymbol{W}_{vi3}^{*\mathrm{T}} \boldsymbol{W}_{vi3}^*\}$ and $\tau_{vij} + d_{vij}$ satisfies $|\tau_{vij} + d_{vij}| \le \bar{\tau}_{vij}$.

Substituting (A4) into (A3) yields

$$\frac{\tilde{V}_i'}{V_i} \boldsymbol{v}_i^{\mathrm{T}} (\boldsymbol{\Delta}_{vi} + \boldsymbol{d}_{vi}) \le \sum_{j=1}^{3} \left(\frac{\tilde{V}_i'^2 v_{ij}^2 \Phi_{vi} \boldsymbol{\varsigma}_{vij}^{\mathrm{T}} \boldsymbol{\varsigma}_{vij}}{2 h_{vi1}^2 V_i^2} + \frac{\tilde{V}_i'^2 v_{ij}^2}{2 h_{vi2}^2 V_i^2} \cdot + \frac{h_{vi1}^2}{2} + \frac{h_{vi2}^2 \bar{\tau}_{vij}^2}{2} \right). \tag{A5}$$

Combining (A2) and (A5), it holds that

$$\tilde{V}_i' \dot{\tilde{V}}_i' \le \lambda_i \tilde{V}_i' \left[\frac{\boldsymbol{v}_i^{\mathrm{T}}}{V_i} \left(\boldsymbol{R}_1^{\mathrm{T}} \boldsymbol{g} + \frac{\boldsymbol{F}_{i0}}{m_i} \right) + \frac{\Phi_{vi} \boldsymbol{v}_i^{\mathrm{T}} \boldsymbol{\Xi}_{vi}}{2 h_{vi1}^2 V_i} + \frac{\boldsymbol{v}_i^{\mathrm{T}} \boldsymbol{v}_i \tilde{V}_i'}{2 h_{vi2}^2 V_i^2} \right] + \tilde{V}_i' \left(\frac{\zeta_{vi} \rho_{Ti} \hat{T}_{xi0}}{1 + a_1 p_1} + \zeta_{vi} \varpi_{vi} \right) - \tilde{V}_i' r_{vi} + \lambda_i \sum_{j=1}^{3} \left(\frac{h_{vi1}^2}{2} + \frac{h_{vi2}^2 \bar{\tau}_{vij}^2}{2} \right). \tag{A6}$$

Define $\beta_{vi} = \frac{1}{\rho_{Ti}}$, $g_{vi} = \beta_{vi} \sup_{t \ge 0} \varpi_{vi}$. Let $\tilde{\Phi}_{vi} = \hat{\Phi}_{vi} - \Phi_{vi}$, $\tilde{\beta}_{vi} = \hat{\beta}_{vi} - \beta_{vi}$, $\tilde{g}_{vi} = \hat{g}_{vi} - g_{vi}$, where $\hat{\Phi}_{vi}$, $\hat{\beta}_{vi}$, $\hat{g}_{vi}$ are the estimations of Φ_{vi}, β_{vi} and g_{vi} respectively. Invoking above definitions yields

$$\tilde{V}_i' \zeta_{vi} \varpi_{vi} \le \rho_{Ti} g_{vi} |\tilde{V}_i'| \zeta_{vi} = \rho_{Ti} \hat{g}_{vi} |\tilde{V}_i'| \zeta_{vi} - \rho_{Ti} \tilde{g}_{vi} |\tilde{V}_i'| \zeta_{vi}. \tag{A7}$$

According to Lemma 3, $\rho_{Ti} \hat{g}_{vi} |\tilde{V}_i'| \zeta_{vi}$ satisfies

$$\rho_{Ti} \hat{g}_{vi} |\tilde{V}_i'| \zeta_{vi} \le \rho_{Ti} (\tilde{V}_i' \hat{g}_{vi} \zeta_{vi} \tanh \left(\frac{\tilde{V}_i' \hat{g}_{vi} \zeta_{vi}}{\varepsilon_{vi}} \right) + 0.2785 \varepsilon_{vi}). \tag{A8}$$

Take the following Lyapunov function candidate:

$$L_1 = \frac{1}{2} \tilde{V}_i'^2 + \frac{1}{2 \gamma_{vi1}} \tilde{\Phi}_{vi}^2 + \frac{\rho_{Ti}}{2 \gamma_{vi2}} \tilde{g}_{vi}^2 + \frac{\rho_{Ti}}{2 \gamma_{vi3}} \tilde{\beta}_{vi}^2, \tag{A9}$$

Using (A6)-(A8) and taking the derivative of (A9), we have

$$\dot{L}_1 \le \tilde{V}_i' \left[\rho_{Ti} \hat{g}_{vi} \zeta_{vi} \tanh \left(\frac{\tilde{V}_i' \hat{g}_{vi} \zeta_{vi}}{\varepsilon_{vi}} \right) + \alpha_{vi} - r_{vi} \right] + \frac{\tilde{V}_i' \zeta_{vi} \rho_{Ti} \hat{T}_{xi0}}{1 + a_1 p_1} - \tilde{V}_i' \left(c_{vi} \tilde{V}_i' + \lambda_i \frac{\tilde{\Phi}_{vi} \boldsymbol{v}_i^{\mathrm{T}} \boldsymbol{\Xi}_{vi}}{2 h_{vi1}^2 V_i} \right) + \frac{\rho_{Ti}}{\gamma_{vi2}} \tilde{g}_{vi} (\dot{\hat{g}}_{vi} - \gamma_{vi2} |\tilde{V}_i'| \zeta_{vi}) + \frac{1}{\gamma_{vi1}} \tilde{\Phi}_{vi} \dot{\hat{\Phi}}_{vi} + \frac{\rho_{Ti}}{\gamma_{vi3}} \tilde{\beta}_{vi} \dot{\hat{\beta}}_{vi} + 0.2785 \varepsilon_{vi} \rho_{Ti}$$

$$+\ \lambda_i \sum_{j=1}^{3}\left(\frac{h_{vi1}^2}{2}+\frac{h_{vi2}^2\bar{\tau}_{vij}^2}{2}\right) \tag{A10}$$

It follows from (33) that

$$\frac{\tilde{V}_i'\zeta_{vi}\rho_{Ti}\hat{T}_{xi0}}{1+a_1p_1}=\frac{-\rho_{Ti}\,(1+a_1)}{1+a_1p_1}\tilde{V}_i'B_{vi}. \tag{A11}$$

Bearing in mind that $-a\tanh(a/\vartheta)\le 0$ with $\forall a\in\Re$ and $\vartheta>0$, we obtain $-\tilde{V}_i'B_{vi}\le 0$. Since $|p_1(t)|\le 1$, one has $1-a_1\le 1+a_1p_1\le 1+a_1$. Invoking Lemma 3 yields

$$\frac{-\rho_{Ti}\,(1+a_1)}{1+a_1p_1}\tilde{V}_i'B_{vi}\le -\rho_{Ti}\tilde{V}_i'\hat{g}_{vi}\zeta_{vi}\tanh\left(\frac{\tilde{V}_i'\hat{g}_{vi}\zeta_{vi}}{\varepsilon_{vi}}\right)$$
$$-\rho_{Ti}\tilde{V}_i'\,(\alpha_{vi}-r_{vi})\,\hat{\beta}_{vi}+0.2785\varepsilon_{vi}\rho_{Ti}. \tag{A12}$$

Noting $-\rho_{Ti}\tilde{V}_i'(\alpha_{vi}-r_{vi})\hat{\beta}_{vi}=-\tilde{V}_i'(\alpha_{vi}-r_{vi})-\rho_{Ti}\tilde{V}_i'\times(\alpha_{vi}-r_{vi})\tilde{\beta}_{vi}$ and substituting (34)-(36), (A12) into (A10) result in

$$\dot{L}_1\le -c_{vi}\tilde{V}_i'^2-\frac{\sigma_{vi1}}{\gamma_{vi1}}\tilde{\Phi}_{vi}\hat{\Phi}_{vi}-\frac{\rho_{Ti}\sigma_{vi2}}{\gamma_{vi2}}\tilde{g}_{vi}\hat{g}_{vi}-\frac{\rho_{Ti}\sigma_{vi3}}{\gamma_{vi3}}\tilde{\beta}_{vi}\hat{\beta}_{vi}$$
$$+0.557\varepsilon_{vi}\rho_{Ti}+\lambda_i\sum_{j=1}^{3}\left(\frac{h_{vi1}^2}{2}+\frac{h_{vi2}^2\bar{\tau}_{vij}^2}{2}\right). \tag{A13}$$

Using Young's inequality gives rise to $-\tilde{\Phi}_{vi}\hat{\Phi}_{vi}\le-\frac{1}{2}\tilde{\Phi}_{vi}^2+\frac{1}{2}\Phi_{vi}^2$, $-\tilde{g}_{vi}\hat{g}_{vi}\le-\frac{1}{2}\tilde{g}_{vi}^2+\frac{1}{2}g_{vi}^2$, $-\tilde{\beta}_{vi}\hat{\beta}_{vi}\le-\frac{1}{2}\tilde{\beta}_{vi}^2+\beta_{vi}^2$. Then (A13) is formulated as

$$\dot{L}_1\le -c_{vi}\tilde{V}_i'^2-\frac{\sigma_{vi1}}{2\gamma_{vi1}}\tilde{\Phi}_{vi}^2-\frac{\rho_{Ti}\sigma_{vi2}}{2\gamma_{vi2}}\tilde{g}_{vi}^2-\frac{\rho_{Ti}\sigma_{vi3}}{2\gamma_{vi3}}\tilde{\beta}_{vi}^2$$
$$+\frac{\sigma_{vi1}}{2\gamma_{vi1}}\Phi_{vi}^2+\frac{\rho_{Ti}\sigma_{vi2}}{2\gamma_{vi2}}g_{vi}^2+\frac{\rho_{Ti}\sigma_{vi3}}{2\gamma_{vi3}}\beta_{vi}^2$$
$$+0.557\varepsilon_{vi}\rho_{Ti}+\lambda_i\sum_{j=1}^{3}\left(\frac{h_{vi1}^2}{2}+\frac{h_{vi2}^2\bar{\tau}_{vij}^2}{2}\right)$$
$$\le -\kappa_{vi}L_2+\chi_{vi}, \tag{A14}$$

where $\kappa_{vi}=\min\{2c_{vi},\sigma_{vi1},\sigma_{vi2},\sigma_{vi3}\}$ and $\chi_{vi}=\frac{\sigma_{vi1}}{2\gamma_{vi1}}\Phi_{vi}^2+\frac{\rho_{Ti}\sigma_{vi2}}{2\gamma_{vi2}}g_{vi}^2+\frac{\rho_{Ti}\sigma_{vi3}}{2\gamma_{vi3}}\beta_{vi}^2+\lambda_i\sum_{j=1}^{3}(\frac{h_{vi1}^2}{2}+\frac{h_{vi2}^2\bar{\tau}_{vij}^2}{2})+0.557\varepsilon_{vi}\rho_{Ti}$.

From (A14), it follows that

$$0\le L_1\le[\frac{\chi_{vi}}{\kappa_{vi}}+L_1(0)]e^{-\kappa_{vi}t}+\frac{\chi_{vi}}{\kappa_{vi}},\quad t\ge 0 \tag{A15}$$

As a result, all the closed-loop signals in translational subsystem are SGUUB. It should be noticed that $\tilde{V}_i'$ can be made arbitrarily small by increasing $c_{vi},\gamma_{vi1},\gamma_{vi2},\gamma_{vi3}$ and meanwhile decreasing h_{vi1}, h_{vi2}, σ_{vi1}, σ_{vi2}, σ_{vi3} and ε_{vi}. Therefore, the speed synchronization tracking error can be made arbitrarily small by appropriate choice of the design parameters. Moreover, the choice of a_1 and a_2 should balance the system performance and the number of triggering events. This will be further shown in the following numerical example.

Next, we prove that our proposed control scheme can avoid Zeno behavior. That is, it should ensure that there exists a $t^*>0$ satisfying $\{t_{k+1}^v-t_k^v\}\ge t^*$. Since $e_{Ti}=\hat{T}_{xi0}(t)-T_{xi0}(t)$, $\forall t\in\{t_{k+1}^v-t_k^v\}$, there exists $\frac{d}{dt}|e_{Ti}|=\mathrm{sign}(e_{Ti})\dot{e}_{Ti}\le|\dot{\hat{T}}_{xi0}|$. From (33), $\hat{T}_{xi0}$ is differentiable and $\dot{\hat{T}}_{xi0}$ is a function of all closed-loop signals. Therefore, there exists a constant μ_{Ti} such that $|\dot{\hat{T}}_{xi0}(t)|\le\mu_{Ti}$. Since $e_{Ti}(t_k^v)=0$ and $\lim_{t\to t_{k+1}^v}e_{Ti}(t)=a_2$, it can be seen that the lower bound of t^* satisfies $t^*\le\mu_{Ti}/a_2$, which means that the Zeno behavior is successfully excluded. This completes the proof of Theorem 1. ■

APPENDIX B
PROOF OF THEOREM 2

Step 1: Choose the following Lyapunov function as

$$L_2=\frac{1}{2}\boldsymbol{e}_{\varphi i}'^{\mathrm{T}}\boldsymbol{e}_{\varphi i}'. \tag{B1}$$

Define $\boldsymbol{e}_{\omega i}=\boldsymbol{\omega}_i-\boldsymbol{\omega}_{di}$. Taking the derivative of (B1) along the trajectories of (16) and (32) arrives at

$$\dot{L}_2=\boldsymbol{e}_{\varphi i}'^{\mathrm{T}}[\lambda_i'\left(\boldsymbol{R}_2^{-1}\boldsymbol{\omega}_{di}+\boldsymbol{R}_2^{-1}\boldsymbol{e}_{\omega i}-\dot{\boldsymbol{\varphi}}_r\right)-\lambda_{i4}\sum_{j\in\mathcal{N}_i}a_{ij}\dot{\boldsymbol{e}}_{\varphi j}], \tag{B2}$$

We design the intermediate controller $\boldsymbol{\omega}_{di}$ as

$$\boldsymbol{\omega}_{di}=\frac{\boldsymbol{R}_2}{\lambda_i'}\left(-\boldsymbol{K}_{1i}\boldsymbol{e}_{\varphi i}'+\lambda_i'\dot{\boldsymbol{\varphi}}_r+\lambda_{i4}\sum_{j\in\mathcal{N}_i}a_{ij}\dot{\boldsymbol{e}}_{\varphi j}\right), \tag{B3}$$

where $\boldsymbol{K}_{1i}\in\Re^{3\times3}$ is symmetric positive definite matrix.

Substituting (B3) into (B2) leads to

$$\dot{L}_2=-\boldsymbol{e}_{\varphi i}'^{\mathrm{T}}\boldsymbol{K}_{1i}\boldsymbol{e}_{\varphi i}'+\lambda_i'\boldsymbol{e}_{\omega i}^{\mathrm{T}}(\boldsymbol{R}_2^{-1})^{\mathrm{T}}\boldsymbol{e}_{\varphi i}'. \tag{B4}$$

Step 2: For the purpose of forcing $\boldsymbol{\omega}_i$ to track $\boldsymbol{\omega}_{di}$, from (22), it holds that

$$\boldsymbol{e}_{\omega i}^{\mathrm{T}}\dot{\boldsymbol{e}}_{\omega i}=\boldsymbol{e}_{\omega i}^{\mathrm{T}}(\boldsymbol{J}_{i0}^{-1}\boldsymbol{S}\left(\boldsymbol{J}_{i0}\boldsymbol{\omega}_i\right)+\boldsymbol{J}_{i0}^{-1}\boldsymbol{N}_{i0}+\boldsymbol{J}_{i0}^{-1}\boldsymbol{C}_{i0}\boldsymbol{\rho}_{\delta i}\boldsymbol{D}_i\hat{\boldsymbol{\delta}}_{i0})$$
$$+\boldsymbol{e}_{\omega i}^{\mathrm{T}}\left(\boldsymbol{\sigma}_i'+\boldsymbol{\Delta}_{\omega i}'+\boldsymbol{l}_{\omega i}+\boldsymbol{d}_{\omega i}-\dot{\boldsymbol{\omega}}_{di}\right), \tag{B5}$$

where $\boldsymbol{\sigma}_i'=\boldsymbol{J}_{i0}^{-1}\boldsymbol{C}_0\boldsymbol{\rho}_{\delta i}\boldsymbol{\sigma}_i$ is bounded.

Using (23) yields

$$\boldsymbol{e}_{\omega i}^{\mathrm{T}}\left(\boldsymbol{\Delta}_{\omega i}'+\boldsymbol{\sigma}_i'+\boldsymbol{l}_{\omega i}+\boldsymbol{d}_{\omega i}\right)=\sum_{j=1}^{3}e_{\omega ij}\boldsymbol{W}_{\omega ij}^{*\mathrm{T}}\boldsymbol{\varsigma}_{\omega ij}+\sum_{j=1}^{3}e_{\omega ij}\cdot$$
$$(\tau_{\omega ij}+\sigma_{ij}'+l_{\omega ij}+d_{\omega ij}). \tag{B6}$$

Using Young's inequality, one has

$$e_{\omega ij}\boldsymbol{W}_{\omega ij}^{*\mathrm{T}}\boldsymbol{\varsigma}_{\omega ij}\le\frac{e_{\omega ij}^2\Phi_{\omega i}\boldsymbol{\varsigma}_{\omega ij}^{\mathrm{T}}\boldsymbol{\varsigma}_{\omega ij}}{2h_{\omega i1}^2}+\frac{h_{\omega i1}^2}{2},$$
$$e_{\omega ij}\left(\tau_{\omega ij}+\sigma_{ij}'+l_{\omega ij}+d_{\omega ij}\right)\le\frac{e_{\omega ij}^2}{2h_{\omega i2}^2}+\frac{h_{\omega i2}^2\bar{\tau}_{\omega ij}^2}{2}, \tag{B7}$$

where $\Phi_{\omega i}=\max\{\boldsymbol{W}_{\omega i1}^{*\mathrm{T}}\boldsymbol{W}_{\omega i1}^*,\boldsymbol{W}_{\omega i2}^{*\mathrm{T}}\boldsymbol{W}_{\omega i2}^*,\boldsymbol{W}_{\omega i3}^{*\mathrm{T}}\boldsymbol{W}_{\omega i3}^*\}$, and the term $(\tau_{\omega ij}+\sigma_{ij}'+l_{\omega ij}+d_{\omega ij})$ satisfies $|\tau_{\omega ij}+\sigma_{ij}'+l_{\omega ij}+d_{\omega ij}|\le\bar{\tau}_{\omega ij}$.

Substituting (B7) into (B6) gives

$$\boldsymbol{e}_{\omega i}^{\mathrm{T}}\left(\boldsymbol{\Delta}_{\omega i}'+\boldsymbol{\sigma}_{i}'+\boldsymbol{l}_{\omega i}+\boldsymbol{d}_{\omega i}\right) \leq \boldsymbol{e}_{\omega i}^{\mathrm{T}}\left(\frac{\Phi_{\omega i}\boldsymbol{\Xi}_{\omega i}}{2h_{\omega i1}^{2}}+\frac{\boldsymbol{e}_{\omega i}}{2h_{\omega i2}^{2}}\right)+\sum_{j=1}^{3}\left(\frac{h_{\omega i1}^{2}}{2}+\frac{h_{\omega i2}^{2}\bar{\tau}_{\omega ij}^{2}}{2}\right). \quad \text{(B8)}$$

Since $\lambda_{\min}(\boldsymbol{J}_{i0}^{-1}\boldsymbol{C}_{i0}\boldsymbol{\rho}_{\delta i}(\boldsymbol{J}_{i0}^{-1}\boldsymbol{C}_{i0})^{\mathrm{T}}) \geq g_{i,\min}$ by Assumption 2, we arrive

$$\lambda_{\min}(\boldsymbol{J}_{i0}^{-1}\boldsymbol{C}_{i0}\boldsymbol{\rho}_{\delta i}\boldsymbol{D}_{i}(\boldsymbol{J}_{i0}^{-1}\boldsymbol{C}_{i0})^{\mathrm{T}}) \geq \frac{g_{i,\min}}{1+b_{1}}>0. \quad \text{(B9)}$$

Define $g_{\omega i}=\inf_{t\geq 0}\lambda_{\min}(\boldsymbol{J}_{i0}^{-1}\boldsymbol{C}_{i0}\boldsymbol{\rho}_{\delta i}\boldsymbol{D}_{i}(\boldsymbol{J}_{i0}^{-1}\boldsymbol{C}_{i0})^{\mathrm{T}})$, $\beta_{\omega i}=\frac{1}{g_{\omega i}}$. Let $\tilde{\Phi}_{\omega i}=\hat{\Phi}_{\omega i}-\Phi_{\omega i}$, $\tilde{\beta}_{\omega i}=\hat{\beta}_{\omega i}-\beta_{\omega i}$ with $\hat{\Phi}_{\omega i}$, $\hat{\beta}_{\omega i}$ being the estimations of $\Phi_{\omega i}$ and $\beta_{\omega i}$ respectively.

Consider the following quadratic function candidate:

$$L_{3}=L_{2}+\frac{1}{2}\boldsymbol{e}_{\omega i}^{\mathrm{T}}\boldsymbol{e}_{\omega i}+\frac{1}{2\gamma_{\omega i1}}\tilde{\Phi}_{\omega i}^{2}+\frac{g_{\omega i}}{2\gamma_{\omega i2}}\tilde{\beta}_{\omega i}^{2}, \quad \text{(B10)}$$

It follows from (B4),(B5) and (B8) that the time derivative of (B10) denotes

$$\begin{aligned}\dot{L}_{3}=&-\boldsymbol{e}_{\varphi i}'^{\mathrm{T}}\boldsymbol{K}_{1i}\boldsymbol{e}_{\varphi i}'-\boldsymbol{e}_{\omega i}^{\mathrm{T}}\boldsymbol{K}_{2i}\boldsymbol{e}_{\omega i}+\boldsymbol{e}_{\omega i}^{\mathrm{T}}\boldsymbol{\zeta}_{\omega i}-\boldsymbol{e}_{\omega i}^{\mathrm{T}}\frac{\tilde{\Phi}_{\omega i}\boldsymbol{\Xi}_{\omega i}}{2h_{\omega i1}^{2}}\\&+\boldsymbol{e}_{\omega i}^{\mathrm{T}}\boldsymbol{J}_{i0}^{-1}\boldsymbol{C}_{i0}\boldsymbol{\rho}_{\delta i}\boldsymbol{D}_{i}\hat{\boldsymbol{\delta}}_{i0}+\sum_{j=1}^{3}\left(\frac{h_{\omega i1}^{2}}{2}+\frac{h_{\omega i2}^{2}\bar{\tau}_{\omega ij}^{2}}{2}\right)\\&+\frac{1}{\gamma_{\omega i1}}\tilde{\Phi}_{\omega i}\dot{\hat{\Phi}}_{\omega i}+\frac{g_{\omega i}}{\gamma_{\omega i2}}\tilde{\beta}_{\omega i}\dot{\hat{\beta}}_{\omega i}, \end{aligned}\quad \text{(B11)}$$

Noting (37) and invoking Lemma 2, it follows that

$$\begin{aligned}&\boldsymbol{e}_{\omega i}^{\mathrm{T}}\boldsymbol{J}_{i0}^{-1}\boldsymbol{C}_{i0}\boldsymbol{\rho}_{\delta i}\boldsymbol{D}_{i}\hat{\boldsymbol{\delta}}_{i0}=-\boldsymbol{e}_{\omega i}^{\mathrm{T}}\boldsymbol{J}_{i0}^{-1}\boldsymbol{C}_{i0}\boldsymbol{\rho}_{\delta i}\boldsymbol{D}_{i}\left(\boldsymbol{J}_{i0}^{-1}\boldsymbol{C}_{i0}\right)^{\mathrm{T}}\cdot\\&\frac{\boldsymbol{e}_{\omega i}\hat{\beta}_{\omega i}^{2}\boldsymbol{\zeta}_{\omega i}^{\mathrm{T}}\boldsymbol{\zeta}_{\omega i}}{\sqrt{\hat{\beta}_{\omega i}^{2}\boldsymbol{e}_{\omega i}^{\mathrm{T}}\boldsymbol{e}_{\omega i}\boldsymbol{\zeta}_{\omega i}^{\mathrm{T}}\boldsymbol{\zeta}_{\omega i}+\varepsilon_{\omega i}}}\leq\frac{-g_{\omega i}\hat{\beta}_{\omega i}^{2}\boldsymbol{e}_{\omega i}^{\mathrm{T}}\boldsymbol{e}_{\omega i}\boldsymbol{\zeta}_{\omega i}^{\mathrm{T}}\boldsymbol{\zeta}_{\omega i}}{\sqrt{\hat{\beta}_{\omega i}^{2}\boldsymbol{e}_{\omega i}^{\mathrm{T}}\boldsymbol{e}_{\omega i}\boldsymbol{\zeta}_{\omega i}^{\mathrm{T}}\boldsymbol{\zeta}_{\omega i}+\varepsilon_{\omega i}}}\\&\leq g_{\omega i}\sqrt{\varepsilon_{\omega i}}-g_{\omega i}|\hat{\beta}_{\omega i}|\,\|\boldsymbol{e}_{\omega i}\|\,\|\boldsymbol{\zeta}_{\omega i}\|\\&\leq g_{\omega i}\sqrt{\varepsilon_{\omega i}}-g_{\omega i}\hat{\beta}_{\omega i}\boldsymbol{e}_{\omega i}^{\mathrm{T}}\boldsymbol{\zeta}_{\omega i}. \end{aligned}\quad \text{(B12)}$$

Substituting (38)-(39) and (B12) into (B11), it holds that

$$\begin{aligned}\dot{L}_{3}\leq&-\boldsymbol{e}_{\varphi i}'^{\mathrm{T}}\boldsymbol{K}_{1i}\boldsymbol{e}_{\varphi i}'-\boldsymbol{e}_{\omega i}^{\mathrm{T}}\boldsymbol{K}_{2i}\boldsymbol{e}_{\omega i}+\boldsymbol{e}_{\omega i}^{\mathrm{T}}\boldsymbol{\zeta}_{\omega i}+g_{\omega i}\sqrt{\varepsilon_{\omega i}}\\&-g_{\omega i}(\hat{\beta}_{\omega i}-\tilde{\beta}_{\omega i})\boldsymbol{e}_{\omega i}^{\mathrm{T}}\boldsymbol{\zeta}_{\omega i}+\sum_{j=1}^{3}\left(\frac{h_{\omega i1}^{2}}{2}+\frac{h_{\omega i2}^{2}\bar{\tau}_{\omega ij}^{2}}{2}\right)\\&-\frac{\sigma_{\omega i1}}{\gamma_{\omega i1}}\tilde{\Phi}_{\omega i}\hat{\Phi}_{\omega i}-\frac{g_{\omega i}\sigma_{\omega i2}}{\gamma_{\omega i2}}\tilde{\beta}_{\omega i}\hat{\beta}_{\omega i}, \end{aligned}\quad \text{(B13)}$$

Following $g_{\omega i}(\hat{\beta}_{\omega i}-\tilde{\beta}_{\omega i})=g_{\omega i}\beta_{\omega i}=1$, one arrives

$$\begin{aligned}\dot{L}_{3}\leq&-\boldsymbol{e}_{\varphi i}'^{\mathrm{T}}\boldsymbol{K}_{1i}\boldsymbol{e}_{\varphi i}'-\boldsymbol{e}_{\omega i}^{\mathrm{T}}\boldsymbol{K}_{2i}\boldsymbol{e}_{\omega i}+\sum_{j=1}^{3}\left(\frac{h_{\omega i1}^{2}}{2}+\frac{h_{\omega i2}^{2}\bar{\tau}_{\omega ij}^{2}}{2}\right)\\&+g_{\omega i}\sqrt{\varepsilon_{\omega i}}-\frac{\sigma_{\omega i1}}{\gamma_{\omega i1}}\tilde{\Phi}_{\omega i}\hat{\Phi}_{\omega i}-\frac{g_{\omega i}\sigma_{\omega i2}}{\gamma_{\omega i2}}\tilde{\beta}_{\omega i}\hat{\beta}_{\omega i}. \end{aligned}\quad \text{(B14)}$$

Using Young's inequality for the terms of $\tilde{\Phi}_{\omega i}\hat{\Phi}_{\omega i}$ and $\tilde{\beta}_{\omega i}\hat{\beta}_{\omega i}$, it can be checked that

$$\dot{L}_{3}\leq-\kappa_{\omega i}L_{3}+\chi_{\omega i}, \quad \text{(B15)}$$

where $\kappa_{\omega i}=\min\{2\lambda_{\min}(\boldsymbol{K}_{1i}),2\lambda_{\min}(\boldsymbol{K}_{2i}),\sigma_{\omega i1},\sigma_{\omega i2}\}$ and $\chi_{\omega i}=g_{\omega i}\sqrt{\varepsilon_{\omega i}}+\sum_{j=1}^{3}(\frac{h_{\omega i1}^{2}}{2}+\frac{h_{\omega i2}^{2}\bar{\tau}_{\omega ij}^{2}}{2})+\frac{\sigma_{\omega i1}}{2\gamma_{\omega i1}}\Phi_{\omega i}^{2}+\frac{g_{\omega i}\sigma_{\omega i2}}{2\gamma_{\omega i2}}\beta_{\omega i}^{2}$.

Integrating (B15) over $[0,\ t]$ leads to

$$0\leq L_{3}\leq\left[\frac{\chi_{\omega i}}{\kappa_{\omega i}}+L_{3}(0)\right]e^{-\kappa_{\omega i}t}+\frac{\chi_{\omega i}}{\kappa_{\omega i}} \quad \text{(B16)}$$

Therefore, it can be seen from (B16) that all closed-loop signals are SGUUB. Note that the convergence region of $\boldsymbol{e}_{\varphi i}'$ can be made smaller by increasing $\boldsymbol{K}_{1i}$, $\boldsymbol{K}_{2i}$, $\gamma_{\omega i1}$, $\gamma_{\omega i2}$ and meanwhile decreasing $h_{\omega i1}$, $h_{\omega i2}$, $\sigma_{\omega i1}$, $\sigma_{\omega i2}$ and $\varepsilon_{\omega i}$. Thus attitude synchronization tracking error can be made as small as desired by appropriate choice of the design parameters. Moreover, the choice of b_1 and b_2 requires to balance the control performance and the number of triggering events. This will be further shown in the following simulations.

Further, it is proved that the Zeno behavior can be avoided. That is to guarantee that there exists a $t^{*}>0$ such that $\{t_{k+1}^{\varphi}-t_{k}^{\varphi}\}\geq t^{*}$. Since $\boldsymbol{e}_{\delta i}=\hat{\boldsymbol{\delta}}_{i0}(t)-\hat{\boldsymbol{\delta}}_{i0}(t_{k}),\forall t\in\{t_{k+1}^{\varphi}-t_{k}^{\varphi}\}$, we obtain $\dot{\boldsymbol{e}}_{\delta i}(t)=\dot{\hat{\boldsymbol{\delta}}}_{i0}(t)$. From (37), $\hat{\boldsymbol{\delta}}_{i0}(t)$ is a function of bounded closed-loop signals. It is clear that $\dot{\boldsymbol{e}}_{\delta i}(t)$ is bounded and $|\dot{e}_{\delta ij}(t)|=|\dot{\hat{\delta}}_{i0j}(t)|\leq\mu_{\delta ij}$ with positive constant $\mu_{\delta ij}$, $j=1,2,3$, where $e_{\delta ij}$ and $\hat{\delta}_{i0j}$ are the jth elements of $\boldsymbol{e}_{\delta i}$ and $\hat{\boldsymbol{\delta}}_{i0}$ respectively. Considering $e_{\delta ij}(t_{k}^{\varphi})=0$ and $\lim_{t\to t_{k+1}^{\varphi}}e_{\delta ij}(t)=b_{2}$, it can be judged that $t^{*}\geq\mu_{\delta ij}/b_{2}$, hence the Zeno behavior is successfully precluded. This completes the proof of Theorem 2. ■

REFERENCES

[1] T. Kim and D. Qiao, "Energy-efficient data collection for IoT networks via cooperative multi-hop UAV networks," *IEEE Trans. Veh. Technol.*, vol. 69, no. 11, pp. 13796–13811, Nov. 2020.

[2] Y. Chen, D. Chang, and C. Zhang, "Autonomous tracking using a swarm of UAVs: A constrained multi-agent reinforcement learning approach," *IEEE Trans. Veh. Technol.*, vol. 69, no. 11, pp. 13702–13717, Nov. 2020.

[3] Y. Wang, M. Shan, and D. Wang, "Motion capability analysis for multiple fixed-wing UAV formations with speed and heading rate constraints," *IEEE Control Netw. Syst.*, vol. 7, no. 2, pp. 977–989, Jun. 2020.

[4] Z. Yu, Y. Zhang, B. Jiang, C. Y. Su, J. Fu, Y. Jin, and T. Chai, "Fractional-order adaptive fault-tolerant synchronization tracking control of networked fixed-wing UAVs against actuator-sensor faults via intelligent learning mechanism," *IEEE Trans. Neural Netw. Learn. Syst.*, vol. 32, no. 12, pp. 5539–5553, Dec. 2021.

[5] M. Lv, B. De Schutter, C. Shi, and S. Baldi, "Logic-based distributed switching control for agents in power chained form with multiple unknown control directions," *Automatica*, 2021, *submitted for publication*.

[6] S. Li and X. Wang, "Finite-time consensus and collision avoidance control algorithms for multiple AUVs," *Automatica*, vol. 49, no. 11, pp. 3359–3367, 2013.

[7] Z. Yu, Y. Zhang, Z. Liu, Y. Qu, and C. Y. Su, "Distributed adaptive fractional-order fault tolerant cooperative control of networked unmanned aerial vehicles via fuzzy neural networks," *IET Control Theory Appl.*, vol. 13, no. 17, pp. 2917–2929, 2019.

[8] Z. Yu, Y. Qu and Y. Zhang, "Distributed fault-tolerant cooperative control for multi-UAVs under actuator fault and input saturation," *IEEE Trans. Control Syst. Technol.*, vol. 27, no. 6, pp. 2417–2429, Nov. 2019.

[9] Y. Wang, T. Zhang, Z. Cai, J. Zhao, and K. Wu, "Multi-UAV coordination control by chaotic grey wolf optimization based distributed MPC with event-triggered strategy," *Chin. J. Aeronaut.*, vol. 33, no. 11, pp. 2877–2897, 2020. [Online]. Available: https://doi.org/10.1016/j.cja.2020.04.028

[10] T. Z. Muslimov and R. A. Munasypov, "Adaptive decentralized flocking control of multi-UAV circular formations based on vector fields and backstepping," *ISA Trans.*, vol. 107, pp. 143–159, 2020. [Online]. Available: https://doi.org/10. 1016/ j.isatra.2020.08.011

[11] L. Xing, C. Wen, Z. Liu, H. Su, and J. Cai, "Event-triggered adaptive control for a class of uncertain nonlinear systems," *IEEE Trans. Autom. Control*, vol. 62, no. 4, pp. 2071–2076, Apr. 2017.

[12] Z. Cai, H. Zhou, J. Zhao, K. Wu, and Y. Wang, "Formation control of multiple unmanned aerial vehicles by event-triggered distributed model predictive control," *IEEE Access*, vol. 6, pp. 55614–55627, Oct. 2018.

[13] N. Hung, A. Pascoal, and T. Johansen, "Cooperative path following of constrained autonomous vehicles with model predictive control and event-triggered communications," *Int. J. Robust Nonlinear Control*, vol. 30, no. 7, pp. 2644–2670, 2020. [Online]. Available: https://doi.org/10.1002/rnc.4896

[14] Z. Wu, J. Xiong, and M. Xie, "A switching method to event-triggered output feedback control for unmanned aerial vehicles over cognitive radio networks," *IEEE Trans. Syst. Man Cybern.-Syst.*, vol. 51, no. 12, pp. 7530–7541, Dec. 2021. [Online]. Available: 10.1109/TSMC.2020.2971726

[15] B. Tian, J. Cui, H. Lu, L. Liu, and Q. Zong, "Attitude control of UAVs based on event-triggered super-twisting algorithm," *IEEE Trans. Ind. Informat.*, vol. 17, no. 2, pp. 1029–1038, Feb. 2021. [Online]. Available: 10.1109/TII.2020. 2981367

[16] H. Yang *et al.*, "Fault-tolerant cooperative control of multi-agent systems: A survey of trends and methodologies," *IEEE Trans. Ind. Informat.*, vol. 16, no. 1, pp. 4–17, Jan. 2020.

[17] M. A. Kamel, X. Yu, and Y. Zhang, "Formation control and coordination of multiple unmanned ground vehicles in normal and faulty situations: A review," *Annu. Rev. Control*, vol. 49, pp. 128–144, 2020.

[18] Z. Yu, Z. Liu, Y. Zhang, Y. Qu, and C. Y. Su, "Distributed finite-time fault-tolerant containment control for multiple unmanned aerial vehicles," *IEEE Trans. Neural Netw. Learn. Syst.*, vol. 31, no. 6, pp. 2077–2091, Jun. 2020.

[19] Z. Yu, Y. Zhang, Z. Liu, Y. Qu, C. Su, and B. Jiang, "Decentralized finite-time adaptive fault-tolerant synchronization tracking control for multiple UAVs with prescribed performance," *J. Franklin Inst.- Eng. Appl. Math.*, vol. 357, no. 16, pp. 11830–11862, 2020. [Online]. Available: https://doi.org/10.1016/j.jfranklin.2019.11.056

[20] Z. Yu, Y. Zhang, B. Jiang, C. Y. Su, J. Fu, Y. Jin, and T. Chai, "Decentralized fractional-order backstepping fault-tolerant control of multi-UAVs against actuator faults and wind effects," *Aerosp. Sci. Technol.*, vol. 104, pp. 105939–105956, Sep. 2020.

[21] C. Liu, B. Jiang, and K. Zhang, "Adaptive fault-tolerant H-infinity output feedback control for leadwing close formation flight," *IEEE Trans. Syst. Man Cybern.-Syst.*, vol. 50, no. 8, pp. 2804–2814, Aug. 2020.

[22] Z. Yu, Y. Zhang, B. Jiang, C. Y. Su, J. Fu, Y. Jin, and T. Chai, "Nussbaum based finite time fractional order backstepping fault tolerant flight control of fixed wing UAV against input saturation with hardware in the loop validation," *Mech. Syst. Signal Process.*, vol. 153, pp. 107406–107425, May 2021.

[23] O. Espen, S. Rune, and K. Raymond, "Underactuated waypoint tracking of a fixed-wing UAV," *IFAC Proc.*, vol. 46, no. 30, pp. 126–133, 2015.

[24] H. Castaneda, O. S. Salas-Pena, and J. Leon-Morales, "Extended observer based on adaptive second order sliding mode control for a fixed wing UAV," *ISA Trans.*, vol. 66, pp. 226–232, 2017.

[25] H. Wang, P. X. Liu, X. Zhao, and X. Liu, "Adaptive fuzzy finite-time control of nonlinear systems with actuator faults," *IEEE Trans. Cybern.*, vol. 50, no. 5, pp. 1786–1797, May 2020.

[26] D. Wang, Q. Zong, B. Tian, S. Shao, X. Zhang, and X. Zhao, "Neural network disturbance observer-based distributed finite-time formation tracking control for multiple unmanned helicopters," *ISA Trans.*, vol. 73, pp. 208–226, 2018.

[27] S. Shao, M. Chen, and Y. Zhang, "Adaptive discrete-time flight control using disturbance observer and neural networks," *IEEE Trans. Neural Netw. Learn. System*, vol. 30, no. 12, pp. 3708–3721, Dec. 2019.

[28] G. Lai, Z. Liu, Y. Zhang, and C. Philip, "Adaptive position/attitude tracking control of aerial robot with unknown inertial matrix based on a new robust neural identifier," *IEEE Trans. Neural Netw. Learn. System*, vol. 27, no. 1, pp. 18–31, Jan. 2016.

[29] S. C. Tong, Y. M. Li, and P. Shi, "Observer-based adaptive fuzzy backstepping output feedback control of uncertain MIMO pure-feedback nonlinear systems," *IEEE Trans. Fuzzy Syst.*, vol. 20, no. 4, pp. 771–785, Aug. 2012.

[30] H. Yang, B. Jiang, H. Yang, and H. H. Liu, "Synchronization of multiple 3-DoF helicopters under actuator faults and saturations with prescribed performance," *ISA Trans.*, vol. 75, pp. 118–126, 2018.

[31] W. Cai, X. Liao, and Y. Song, "Indirect robust adaptive fault-tolerant control for attitude tracking of spacecraft," *J. Guid. Control Dyn.*, vol. 31, no. 5, pp. 1456–1463, 2008.

[32] W. Liu, Y. Geng, B. Wu, and D. Wang, "Neural-network-based adaptive event-triggered control for spacecraft attitude tracking," *IEEE Trans. Neural Netw. Learn. Syst.*, vol. 31, no. 10, pp. 4015–4024, Oct. 2020. [Online]. Available: 10.1109/TNNLS.2019.2951732

[33] M. Lv, W. Yu, J. Cao, and S. Baldi, "A separation-based methodology to consensus tracking of switched high-order nonlinear multi-agent systems," *IEEE Trans. Neural Netw. Learn. Syst.*, to be published, doi: 10.1109/TNNLS.2021.3070824.

[34] M. Lv, W. Yu, J. Cao, and S. Baldi, "Consensus in high-power multi-agent systems with mixed unknown control directions via hybrid Nussbaum-based control," *IEEE Trans. Cybern.*, to be published, doi: 10.1109/TCYB.2020.3028171.

[35] L. Xing, C. Wen, Y. Zhu, H. Su, and Z. Liu, "Output feedback control for uncertain nonlinear systems with input quantization," *Automatica*, vol. 65, pp. 191–202, 2016.

[36] E. Cruz-Zavala, J. Moreno, and L. Fridman, "Uniform robust exact differentiator," *IEEE Trans. Autom. Control*, vol. 56, no. 11, pp. 2727–2733, Nov. 2011.